Journal of Molecular Liquids 382 (2023) 121943

Contents lists available at ScienceDirect

Journal of Molecular Liquids

journal homepage: www.elsevier.com/locate/molliq

Diffusion coefficient and the volume swelling of CO_2/light oil systems: Insights from dynamic volume analysis and molecular dynamics simulation

Yongcheng Luo [a,b,c], Hanmin Xiao [b,c,*], Xiangui Liu [b,c], Taiyi Zheng [a,d,*], Zhenkai Wu [a,b,c]

[a] College of Engineering Science, University of Chinese Academy of Sciences, Beijing 100049, China
[b] Institute of Porous Flow and Fluid Mechanics, University of Chinese Academy of Sciences, Langfang 065007, China
[c] Research Institute of Petroleum Exploration & Development, Beijing 100083, China
[d] Institute of Mechanics, Chinese Academy of Science, Beijing 100190, China

ARTICLE INFO

Keywords:
CO_2-light oil system
Diffusion coefficient
Swelling factor
Molecular dynamics simulation

ABSTRACT

The oil volume expansion and CO_2 diffusion are one of the main mechanism of CO_2-enhanced oil recovery (CO_2-EOR). This paper established a series of experiments, numerical simulations, and molecular dynamics (MD) simulations to describe mass transfer behaviors between oil–gas phases. Expressly, the CO_2 diffusion coefficient and light oil swelling factor are signification parameters to quantify and analyze these behaviors. In detail, the CO_2 diffusion coefficient and the oil swelling factor were obtained from the traditional pressure decay method and the advanced MD simulation. Synthetically, the pressure decay method and MD simulation results were mutually verified. The results showed that the equilibrium pressure was proportional to the mole fraction of CO_2 and inversely proportional to the mole fraction of light oil. The equilibrium time was proportional to the mole fraction of CO_2 and light oil. At the temperature of 333.15 K and the initial pressure of 7.5 MPa, the CO_2 diffusion coefficient in light oil was positively correlated with the relative molar proportion of CO_2, while the light oil swelling factor was vice versa. In addition, the closer to the CO_2-light oil interface, the greater the light oil's potential energy and self-diffusion coefficient, and the stronger the transport ability.

1. Introduction

In recent years, the tight oil has become the main development resource as the energy solution [1–3]. CO_2 has been broadly applied in tight oil reservoirs as a gas injection medium to enhance oil recovery (EOR) [4–6]. The CO_2-EOR mechanism is mainly realized through oil volume expansion and CO_2 diffusion [7,8]. Expressly, the CO2 diffusion coefficient and oil swelling factor are significant parameters to analyze and quantify these mechanisms.

The CO_2 diffusion coefficient and oil swelling factor are universally obtained by matching the curves of pressure and the oil–gas interface position over time from traditional pressure decay test [9]. In particular, the simulation considering oil–gas interface position variation is optional for heavy oil system [10], but crucial for light oil system. Inheriting this method, Tharanivasan et al. [11] optimized the diffusion coefficient calculation process through the minimum objective function determined by the minimum average difference between laboratory pressure and theoretical pressure. Guo et al. [12] and Ahmadi et al. [13] established a mutual diffusion model by combining diffusion equation and material balance equations for better results. Whereas, the fitting results of most studies focus on the pressure decay process and ignore the pressure equilibrium period. For crude oil volume expansion, Sun et al. [14] manifested this phenomenon based on the modified Peng Robinson (PR) equation. To make the simulation results more accurate, Liu et al. [15] introduced a moving mesh technique with constant mesh number and variable mesh size into the mass transfer model of the CO_2-oil system. However, the researchers only adopted the simulation method without verifying the model's accuracy.

In recent years, molecular dynamics (MD) simulation has gradually become another new way to obtain the above parameters due to its low cost and simulability of complex systems. In addition, the MD simulation has been widely accepted to discern mass transfer in CO_2-oil systems at the microscopic level. In bulk phase condition, Liu et al. [16] andMehana et al. [17] used MD simulation to analyze volume expansion and diffusion mechanism in CO_2-alkanes (hexane, cyclohexane, octane, decane, aromatics, and asphaltenes, etc.) system. Furthermore, using MD simulation, Li et al. [18] investigated the effect of carbon chain

* Corresponding authors at: Institute of Porous Flow and Fluid Mechanics, University of Chinese Academy of Sciences, Langfang 065007, China (H. Xiao); Institute of Mechanics, Chinese Academy of Science, Beijing 100190, China (T. Zheng).
E-mail addresses: xiaohm69@petrochina.com.cn (H. Xiao), zhengtaiyi@imech.ac.cn (T. Zheng).

https://doi.org/10.1016/j.molliq.2023.121943
Received 5 August 2022; Received in revised form 4 April 2023; Accepted 25 April 2023
Available online 29 April 2023

Nomenclature

a	attraction parameter in the PR EOS model, kPa•m^3/kmol
a_c	factor in correlation of attraction parameter in the PREOS model
b	van der Waals volume, m^3/kmol
c_{CO_2}	concentration of CO_2 in light oil, mol/m^3
c_{eq}	Equilibrium concentration of CO_2 in light oil, mol/m^3
D_{CO_2}	diffusion coefficient of CO_2 in oil phase, m^2/s
h	coordinate direction of liquid phase, m
$H_{g-o}(t)$	the time-dependent position of gas-oil interface, m
m_1, m_2	dimensionless parameter
MW	MWmolar weight
OF	objective function
P	pressure, kPa
P_c, P_{ci}	critical pressure and critical pressure of ith component, respectively, kPa
P^{cal}, P^{exp}	measured pressure and calculated pressure, respectively, kPa
R	universal gas constant, kPa•m^3/(K •kmol)
SF	swelling factor
SG	specific gravity
t	time, s
t_0, t_1	time of 0 and total time, respectively, s
T	temperature, K
T_c	critical temperature, K
T_{ci}, T_{cj}, T_{ck}	critical temperature of component ith, jth and kth component, respectively, K
T_r, T_r^*	reduced temperature and reduced temperature calculated at 288.7 K, respectively, K
V	molar volume, m^3/kmol
V_0	molar volume of light oil at test temperature and initial pressure, m^3/kmol
V_m, V_c	molar volume and critical molar volume, respectively, m^3/kmol
V_{ci}, V_{cj}, V_{ck}	critical molar volume of ith, jth and kth component, respectively, m^3/kmol
V_i'	molar volume correction of the jth component
x_i, x_j	mole fraction of the ith and jth component, respectively, mole fraction
Z_c, Z_{ci}	compression factor of pseudo components and ith component, respectively
Z_{RA}	Rackett parameter

Greek symbols

α	alpha function in PR EOS model
ω	acentric factor
ω_i, ω_j	acentric factor of ith and jth component, respectively
δ_{ij}	BIP of ith and jth
Δh	space interval

length, pressure and temperature on CO_2 solubility and oil swelling coefficient in a series of CO_2-n-alkane systems. Zhang et al. [19], Omrani et al. [20] and Zhao et al. [21] used molecular dynamics simulations to calculate the CO_2 self-diffusion coefficient in different liquids. However, in most MD simulations, the oil phase was only constructed by one class of alkane molecules, which could not fairly represent a multi-component crude oil system. Given this situation, according to Baken oilfield data, Li et al. [22] established a multi-component oil system to study mass transfer behaviors in MD simulation. Defectively, C1-C4 molecules remarkably contained in crude oil were ignored in the model, which also significantly influenced on the oil properties. Besides, the results of existing MD simulations still need experimental validation.

In this paper, we investigated the mass transfer behaviors of the CO_2-light oil system via a series of experiments, numerical simulations, and molecular dynamics simulations. Explore different diffusion processes and simulate the neglected equilibrium diffusion stage. The CO_2 diffusion coefficient in the light oil system was calculated by fitting the pressure–time variation curve of the light oil–gas system by the gas–liquid mass transfer equation. The modified PR-EOS equation was used to characterize the light oil phase swelling effect. At the same time, the MD simulation method was used to calculate the CO2 molecular diffusion coefficient and light oil swelling coefficient, considering the light molecules C1-C4 ignored by predecessors. The experimental, PR-EOS, and molecular dynamics results were compared in oil swelling factor, CO_2 diffusion coefficient and CO_2 concentration distribution. In addition, after CO_2 diffusion in light oil, the potential energy and self-diffusion coefficient of light oil at different positions were calculated. Synthetically, the experiment, numerical, and MD simulation results were mutually verified, which could provide a reliable theoretical basis for exploiting of light oil.

2. Experimental materials and procedure

2.1. Materials

The light oil is the crude oil with large amounts of $C_1 \sim C_{14}$ and small amounts of asphaltene [23,24]. Laboratorial oil was the light oil received from the Chang7 oilfield, China, which belonged to light oil [25]. The density of light oil was 0.8230 g/cm^3 at the ground condition and 0.7428 g/cm^3 at formation condition. Fig. 1 shows the hydrocarbon component distribution in light oil. Besides, laboratory gas was 99.9 mol % CO_2.

In this study, the 5 sets of tests were conducted according to the molar ratio of experimental materials. The initial light oil volume and CO_2 volume are listed in Table 1. In addition, we normalized the molar ratio of light oil to calculate the relative molar amount of CO_2.

2.2. Experimental equipment

As demonstrated in Fig. 2, all CO_2 diffusion processes were tested in the Pressure/Volume/Temperature (PVT) setup. Therein, the PVT-cell with variable volume was the workplace for the diffusion process. It had an inner diameter of 3.0 cm and a maximum volume of 270 mL. At the bottom of the PVT-cell was a transparent glass, which could observe the scene in the PVT-cell through the camera placed outside the PVT-

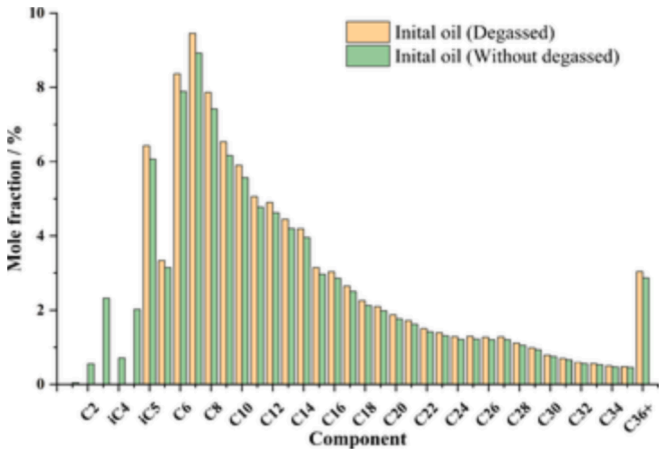

Fig. 1. Mole ratio distribution of oil components.

Table 1
Initial Test sample compositions.

EN	MR CO_2:Oil	RM of CO_2 (Oil = 1)	CO_2 P/ MPa	V/mL	V of Oil /mL	T/℃
#1	0.30:0.10	3.0	5.0	134.31	23.77	59.95
#2	0.30:0.20	1.5	5.0	134.31	47.54	60.01
#3	0.30:0.25	1.2	5.0	134.31	59.42	60.00
#4	0.40:0.10	4.0	5.0	179.08	23.77	60.01
#5	0.40:0.15	2.667	5.0	179.08	35.65	59.95

Note: EN-Experiment number; MR CO_2:Oil-Molar ratio of CO_2:Oil; RM-Relative moles; P-Pressure; V-Volume; T- Temperature.

cell. Additionally, the captured images could monitor the liquid volume in real-time. Moreover, the pressure and temperature measurement accuracy was 0.01 MPa and 0.01℃, respectively.

2.3. Experimental procedure

The pressure-decay test steps of PVT equipment were as follows:

(1) Clean and dry the PVT equipment, and raise the temperature of the experimental test system to 60 °C (±0.1 °C) (maintain for 24 h to ensure constant temperature).
(2) Inject CO_2 into the PVT cylinder and fix the volume of the PVT cylinder. Then, keep the temperature of the test system at 60 °C (±0.1 °C) for 2 h and adjust the amount of CO_2 until the pressure remains constant at 5 MPa.
(3) Quickly inject the light oil preheated to 60 °C into the PVT cylinder from the bottom. Then, increase the pressure to the experimental design value (7.5Mpa) and keep the volume of PVT cylinder constant. Immediately, record the changes of experimental parameters such as pressure with time until the end of the test.

3. Mathematical formulations

The actual CO_2 diffusion process in the CO_2-light oil system was simplified to the physical model described in Fig. 3, where the height of the CO_2-light oil interface was h(t). Notably, h(t) would increase gradually since the light oil volume phase expanded during CO_2 diffusion process. The mass transfer simulation process of CO_2-light oil system was shown in Fig. 4.

3.1. Assumptions

In order to accurately simulate the CO_2 diffusion behavior, the following assumptions were established in the mass transfer model:

(1) The temperature was constant in the CO_2-light oil system during the diffusion process.
(2) Mass transfer resistance did not exist near the vicinity of the gas–liquid interface, where the concentrations of different components were invariably set as equilibrium concentrations [26–29].
(3) z-factor was assumed as a constant in each individual time step, which would be updated in the following time step. Distinctively,

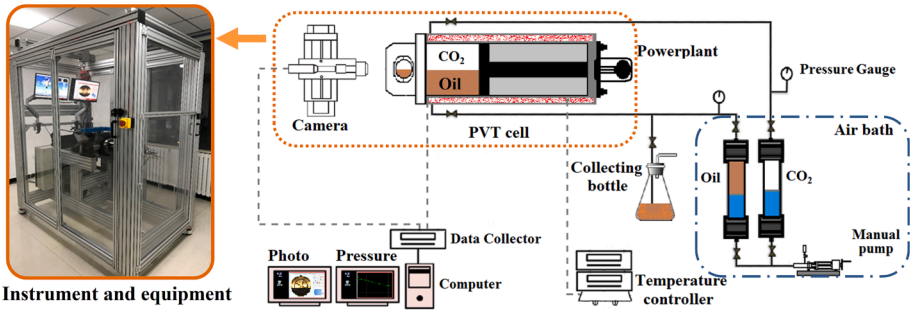

Fig. 2. Schematic of PVT experiment device.

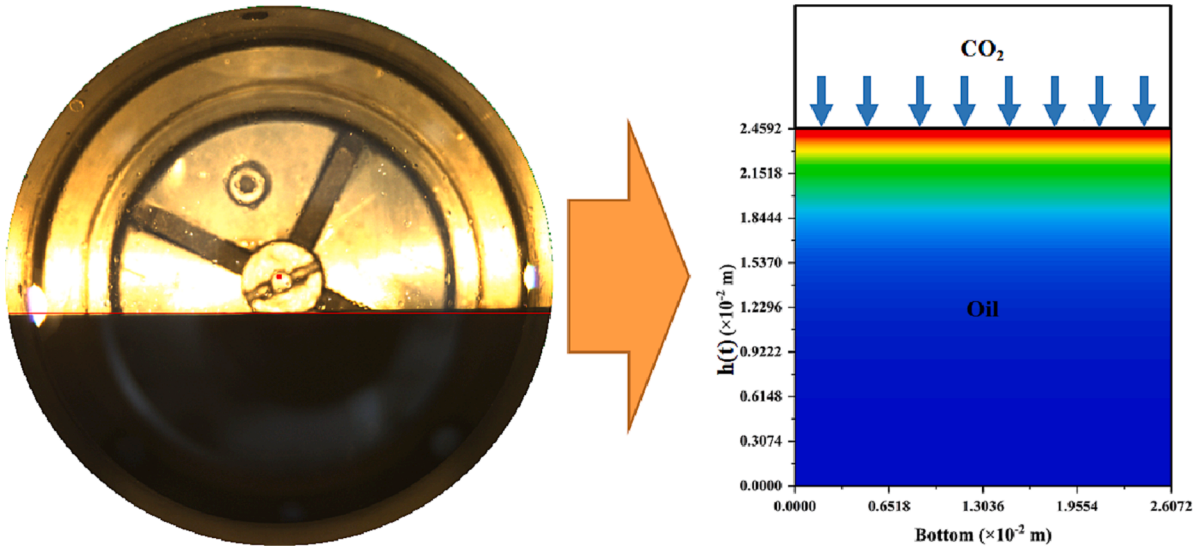

Fig. 3. The schematic of CO_2 diffusion process in CO_2-light oil system.

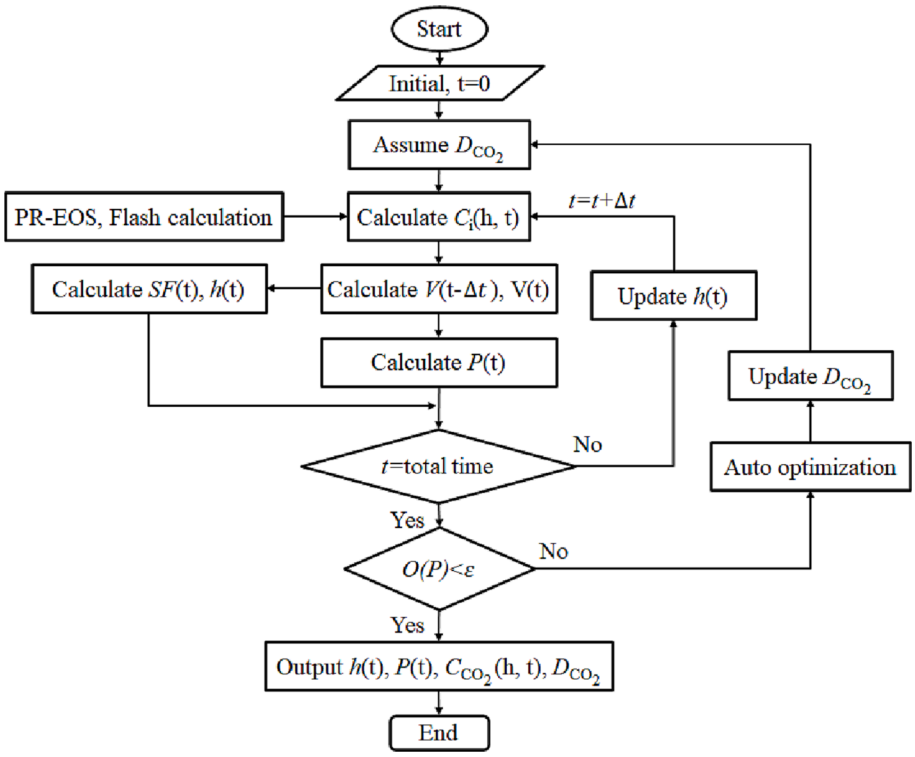

Fig. 4. Flowchart for determining diffusion coefficients and swelling factor in CO_2-light oil system.

CO_2 diffusion coefficient was fixed as a constant (D_{CO_2}) throughout the entire simulation process.

(4) The natural convection was negligible in the CO_2-light oil system.

3.2. Light oil characterization

The light oil components were relatively heterogeneous from previous analysis results, with carbon atoms at 1 to 36. Thus, it was significant to artificially merge several original oil components into a single pseudo-component before simulation to minimize the computational cost. Applying Key's addition rule to calculate the critical pressure of fresh pseudo-components frequently resulted in obvious errors [30]. Therefore, the pseudo-components' critical properties were decided using rules of Lee and Kesler in this paper [30].

$$V_{ci} = \frac{Z_{ci} R T_{ci}}{P_{ci}} \tag{1}$$

$$Z_{ci} = 0.2905 - 0.085\omega_i \tag{2}$$

$$V_c = \frac{1}{8}\sum_j\sum_k x_i x_j \left(V_{cj}^{\frac{1}{3}} + V_{ck}^{\frac{1}{3}}\right)^3 \tag{3}$$

$$T_c = \frac{1}{8V_c}\sum_j\sum_k x_i x_j \left(V_{cj}^{\frac{1}{3}} + V_{ck}^{\frac{1}{3}}\right)^3 \bullet \sqrt{T_{cj}T_{ck}} \tag{4}$$

$$\omega = \sum_j x_j \omega_j \tag{5}$$

$$P_c = \frac{Z_c R T_c}{V_c} = (0.2905 - 0.085\omega)\frac{RT_c}{V_c} \tag{6}$$

Based on the pseudo-component samples proposed by Hawthorne et al. [31], the hydrocarbon components in oil were grouped into 5 pseudo-components, whose correlative properties were shown in Table 2. Moreover, as for the binary interaction parameter (BIP) between different components, the modified Chueh–Prausnitz(7) [32] correlation was found to accurately estimate BIPs of the solvent-enriched oil systems [33,34]。The BIPs applied in simulation were listed in Table 3.

$$\delta_{ij} = m_1\left\{1 - \left[\frac{2\left(V_{ci}V_{cj}\right)^{1/6}}{\left(V_{ci}\right)^{1/3} + \left(V_{cj}\right)^{1/3}}\right]^{m_2}\right\} \tag{7}$$

3.3. Molecular diffusion

Based on Fick's second law, the one-dimensional molecular diffusion model of CO_2-light oil system was described as eq. (8) [35,36]:

$$\frac{\partial c_{CO_2}(h,t)}{\partial t} = D_{CO_2}\frac{\partial^2 c_{CO_2}(h,t)}{\partial x^2} 0 < h < H_{g-o}(t) t_0 < t < t_1 \tag{8}$$

Table 2
Physical properties of pseudo components (PC).

Component	Merge content	Molar fraction /%	Pc, kPa	Tc, K	Vc	Z	Acentric factor
CO_2	CO_2	100.00	7376.46	304.21	0.0940	0.2736	0.2250
PC_1	$C_1 \sim C_4$	5.656	4068.84	388.98	0.2217	0.2752	0.1631
PC_2	$C_5 \sim C_7$	26.019	3272.68	505.16	0.3425	0.2699	0.2723
PC_3	$C_8 \sim C_{13}$	32.734	2449.89	625.29	0.5287	0.2596	0.4437
PC_4	$C_{14} \sim C_{24}$	23.704	1611.74	757.08	0.9129	0.2482	0.7460
PC_5	$C_{25} \sim C_{36+}$	11.887	1173.42	902.93	1.3052	0.2339	1.0241

Table 3
BIP matrix for CO_2-light oil systems.

Component	CO_2	PC_1	PC_2	PC_3	PC_4	PC_5
CO_2	0	0.04369	0.09607	0.16402	0.26463	0.33537
PC_1	0.04369	0	0.01144	0.04479	0.11382	0.17189
PC_2	0.09607	0.01144	0	0.01140	0.05659	0.10244
PC_3	0.16402	0.04479	0.01140	0	0.01798	0.04833
PC_4	0.26463	0.11382	0.05659	0.01798	0	0.00775
PC_5	0.33537	0.17189	0.10244	0.04833	0.00775	0

Initial and Boundary Conditions:
Initial conditions,

$$c_{CO_2}(h,t) = 0, 0 < h < H_{g-o}(t), t = t_0 = 0,$$

Boundary conditions,

$$\frac{\partial c_{CO_2}(h,t)}{\partial h} = 0, h = H_{g-o}(t), t > t_1$$

$$c_{CO_2}(h,t) = c_{eq}, h = H_{g-o}(t) t_0 < t < t_1$$

3.4. Volume-translated PR EOS

Peng Robinson equation of state (PR EOS), eq. (9) is one of the most established and broadly applied flash calculation methods. As an illustration, Sun et al. [14] and Zheng et al. [34] studied the mass transfer of C_3H_8–CO_2 mixture in heavy oil system by PR EOS equation. Similarly, Dong et al. [36] and Zheng et al. [33] used PR EOS equation to describe the mass transfer behavior of CO_2-N_2 mixture in light oil system. Therefore, in this paper, PR EOS was selected to research phase behaviors in this paper due to its simplicity and accuracy.

PR EOS was expressed as [37,38]:

$$P = \frac{RT}{V_m - b} - \frac{a}{V_m(V_m + b) + b(V_m - b)} \tag{9}$$

$$a = a_c \alpha(T_r, \omega) \tag{10}$$

$$a_c = \frac{0.457235 R^2 T_c^2}{P_c} \tag{11}$$

$$b = \frac{0.0777969 R T_c}{P_c} \tag{12}$$

Alpha function was related to whether the phase behaviors could be accurately simulated. Li et al. [39] found that the following alpha function could suitably describe the phase behaviors of two pure substances. Meanwhile, this alpha function had also been applied to multi-pseudo-components system with promising results [14,33,40,41]. Hence, the above alpha function continued to be applied in this paper.

$$\alpha(T_r, \omega) = \exp\left\{ \begin{array}{c} (0.13280 - 0.05052\omega + 0.25948\omega^2)(1 - T_r) \\ +0.81769 ln\left[1 + (0.31355 + 1.86745\omega - 0.52604\omega^2)\left(1 - \sqrt{T_r}\right)\right]^2 \end{array} \right\} \tag{13}$$

For a mixture system, the parameters a and b of the PR equation could be acquired from van der Waals mixing rule [14,33].

$$a = \sum_{i=1}^{nc} \sum_{j=1}^{nc} x_i x_j (1 - \delta_{ij}) \sqrt{a_i a_j} \tag{14}$$

$$b = \sum_{i=1}^{nc} x_i b_i \tag{15}$$

3.5. Dynamic swelling factor and volume translation

CO_2 can effectively dissolve into oil and then cause it to expand, which is an essential mechanism of CO_2 EOR [42–46]. Campos et al. [47] and Lashkarbolooki et al. [48] pointed out that the swelling factor of oil mainly depended on the oil compositions and the CO_2 content. Forming CO_2-oil systems with 9 types of crude oil, Simon and Graue [49] plotted the swelling factor plate for mixture system. Since CO_2 diffusion in oil was a dynamic process approaching equilibrium, swelling factor (eq. (16)) was adopted to quantify the dynamic volume variation of oil phase.

$$SF(t) = \frac{V_{corr}}{V_0} \frac{1}{1 - \frac{\sum_1^{nc_g} \left(\int_0^{H(t)} \Delta A x_i dx \right)}{\sum_1^{nc} \left(\int_0^{H(t)} \Delta A x_i dx \right)}} \tag{16}$$

V_{corr}, the corrected molar volume, was consistent with the modification method proposed by peneloux et al. [38].

$$V_{corr} = V_0 - \sum_i x_i C_i \tag{17}$$

$$C_i = 0.40768 \left(\frac{RT_c}{P_c} \right) (0.29441 - Z_{RA}) \tag{18}$$

The Rackett Parameter could be estimated by the following formula [36,50]:

$$Z_{RA} = \left(\frac{MW \cdot P_c}{SG \cdot R \cdot T_c} \right)^{\frac{1}{1 + (1 - T_r^*)^{2/7}}} \tag{19}$$

3.6. Numerical solution and calculation procedure

The partial differential equations (eq. (21)) of the Fick's second law (eq. (20)) were solved with the finite volume method (FVM) in this study [14,36].

$$\frac{\partial c_o(h,t)}{\partial t} = D_o \frac{\partial^2 c_o(h,t)}{\partial h^2} 0 < h < H_{g-o}(t) t_0 < t < t_1 \tag{20}$$

$$\frac{\partial^2 c_o(h,t)}{\partial h^2} = \frac{C_o(h + \Delta h, t) - 2C_o(h,t) + C_o(h - \Delta h, t)}{(\Delta h)^2} \tag{21}$$

For the solution of the PR EOS, it was transformed into a univariate

cubic equation about the compressibility coefficient Z.

$$V_m = \frac{ZRT}{P} \tag{22}$$

$$Z^3 + (B-1)Z^2 + \left(A - 3B^2 - 2B\right)Z - \left(AB - B^2 - B^3\right) = 0 \tag{23}$$

$$A = \frac{aP}{R^2T^2}, B = \frac{bP}{RT} \tag{24}$$

Particle Swarm Optimization (PSO) proposed by Eberhart and Kennedy in 1995 is an essential representative of swarm intelligence technology [51]. The values of CO_2 diffusion coefficient were tuned with the PSO algorithm for each set of fitting processes to achieve the minimum deviation between experimental and theoretical pressures. The objective function can be expressed as:

$$OF = \sqrt{\frac{1}{N_{exp}}\sum_{1}^{N_{exp}}\left(\frac{P_i^{cal} - P_i^{exp}}{P_i^{exp}}\right)^2} \tag{25}$$

4. Molecular simulation

4.1. Self-diffusion, Maxwell-Stefan (MS) diffusion and Fick diffusion coefficient

Diffusion mass transfer is a phenomenon in which a component in a system migrates due to the concentration gradient, which controls the mixing rate of oil and gas [52]. It is a crucial development parameter for oil and gas reservoirs, especially for tight unconventional reservoirs with low permeability [53]. Therefore, it is necessary to predict the molecular diffusion rate. + At present, self-diffusion, Maxwell-Stefan (MS) Diffusion, and Fick diffusion are frequently used for diffusion coefficients. Among them, the self-diffusion is derived from the random Brownian motion generated by collisions in the mixture [54,55]. In contrast, MS diffusion is the equilibrium result of molecular friction and intermolecular interactions [56,57]. Fick's diffusion is an intuitive definition of net mass transport. In industry, the Fick diffusion coefficient is widely used due to its experimental validity on the concentration gradient of mixtures [58]. Both Fick and MS diffusion coefficients are common or mutual, which can be related by thermodynamic factors [59–61].

4.1.1. Self-diffusion coefficient

In order to precisely obtain the CO_2 self-diffusion coefficient (D_s), the mean square displacement (MSD) [22,62] analytical method was adopted in this paper, which was a technique for determining particle displacement over time [63]. Based on the linear Einstein relation between MSD and diffusion time, the diffusion coefficient can be calculated according to the slope of linear equation (eq. (27)).

$$MSD(\Delta t) = \frac{1}{\tau - \Delta t}\int_0^{\tau-\Delta t}[r(t-\Delta t) - r(t)]^2 dt = \langle [r(t-\Delta t) - r(t)]^2 \rangle \tag{26}$$

$$D_{i,S} = \frac{1}{6N_i}\lim_{t\to\infty}\frac{d}{dt}\langle\sum_{i=1}^{N}[\vec{r_i}(t) - \vec{r_i}(0)]^2\rangle \tag{27}$$

Where τ was the total simulation time, s; *MSD* was the mean square displacement, m^2; $r(t)$, $r(t-\Delta t)$ were the position at t time and the position at $t-\Delta t$, m; $\vec{r_i}$ was the displacement vector of the i-th molecule at time t, m; $D_{i,S}$ was self-diffusion coefficient of particle i, m^2/s; N_i was the number of diffusion molecules.

4.1.2. Maxwell-Stefan diffusion coefficient

At constant temperature and pressure, the MS diffusion coefficient indicates that the driving force of the diffusion process is the chemical potential gradient, which is in equilibrium with the frictional force. The definition of Maxwell-Stefan diffusion coefficient is as follows [56,57,61].

$$-\frac{1}{RT}\nabla\mu_i = \sum_{j=1,j\neq i}^{N_j}\frac{x_j(u_i - u_j)}{D_{ij,MS}} \tag{28}$$

where R is the universal gas constant, T is temperature in Kelvin. $\nabla\mu_i$ is the chemical potential gradient. x_j is the mole fraction of species j. (u_i-u_j) is the difference of average velocity of species i and j. $D_{MS,ij}$ is the M−S diffusivity of the *i-j* pair in the mixture. MS diffusion coefficient is independent of reference frame ($D_{ij,MS} = D_{ji,MS}$).

In molecular dynamics simulations, MS diffusion coefficients cannot be calculated directly. There are three methods that can be used to calculate the MS diffusion coefficient indirectly.

Firstly, the MS diffusion coefficients can be obtained from the Onsager coefficients Λij, and their relationship is shown in eq. 29 and eq. 30 [59,61].

$$\Lambda_{ij} = -\lim_{t\to\infty}\left\{\frac{1}{6Nt}\left\langle\left(\sum_{l=1}^{N_i}\left[\vec{r}_{l,i}(t) - \vec{r}_{l,i}(0)\right]\right)\bullet\left(\sum_{k=1}^{N_j}\left[\vec{r}_{k,j}(t) - \vec{r}_{k,j}(0)\right]\right)\right\rangle\right\} \tag{29}$$

$$D_{12,MS} = \frac{x_2}{x_1}\Lambda_{11} + \frac{x_1}{x_2}\Lambda_{22} - 2\Lambda_{12} \tag{30}$$

Secondly, the MS diffusivity can be obtained from the Darken relation [64,65].

$$D_{ij,MS} = x_i D_{i,S} + x_j D_{j,S} \tag{31}$$

Thirdly, the Vignes-type equation is another way to describe the MS diffusion coefficient in terms of concentration [65,66].

$$D_{ij,MS} = \left(D_{ij,MS}^{x_i\to 1}\right)^{x_i}\left(D_{ij,MS}^{x_j\to 1}\right)^{x_j} \tag{32}$$

4.1.3. Fick diffusion coefficient

The Fick diffusion coefficient is defined according to the gas concentration gradient in the medium. That is, the diffusion flux is negatively related to the concentration gradient of the diffusion process, as expressed by eq. (33) [59,60,61].

$$\vec{J} = -D_F \bullet \nabla c \tag{33}$$

Where D_F is Fick diffusion coefficient, m^2/s; c is concentration, mol/m^3.

From the perspective of thermodynamics, Fick's first law can be expressed as [60,67]:

$$\vec{J} = -\frac{L(c)}{k_B T}\bullet\nabla\mu = -D_{MS}\bullet\nabla\mu \tag{34}$$

The thermodynamic correction factor Γ [59,65]

$$\Gamma = \delta + x_i\left(\frac{\partial ln\gamma_i}{\partial x_i}\right)_{T,p,\Sigma} \tag{35}$$

$$\nabla\mu = \Gamma\nabla c \tag{36}$$

$$D_F = D_{MS}\bullet\Gamma \tag{37}$$

4.2. Models and methods

Fig. 5(a) expressed the molecules and conceptual light oil used in the simulation. Wherein, molecules C_6, C_{10}, C_{19}, C_{30} respectively represented the previous pseudo-components PC_2, PC_3, PC_4, PC_5. A quaternary system (C_6 + C_{10} + C_{19} + C_{30}) to represent the light oil has been successfully used for estimating the minimum miscible pressure (MMP) of the CO_2-Bakken oil system [68]. And Li et al. [22] used the crude oil model to calculate the CO_2 solubility, the CO_2 diffusion coefficient and the crude oil swelling factor. The number of various molecules in light oil was formulated according to the molar composition of light oil in

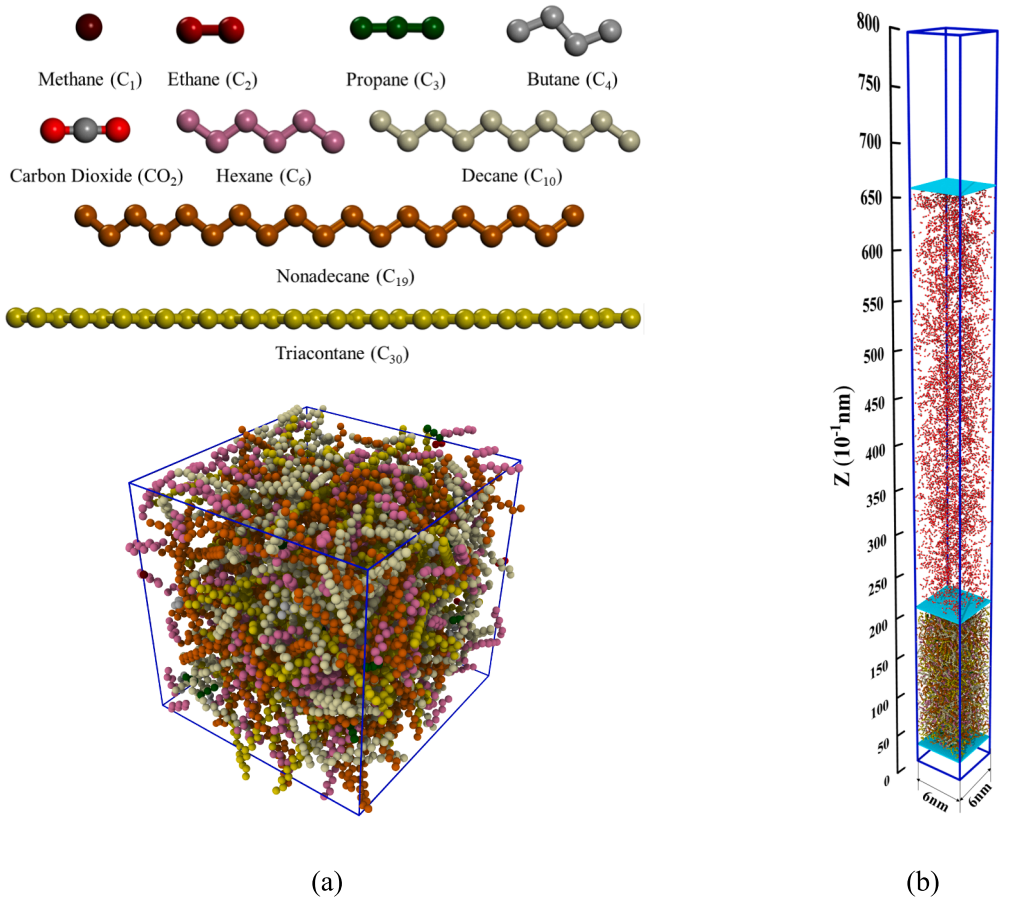

Fig. 5. Schematic diagram of crude oil molecular model: (a) CO_2, crude oil and its components models, (b) CO_2 and light oil simulation system.

Fig. 6, the number of molecules of CO_2 was calculated according to the mole ratio in experiment #1. As illustrated in Fig. 5(b), the CO_2-light oil system was prepared to diffuse in a rectangular lattice of 60 × 60 × 400Å. In addition to increasing the system pressure, three He nanoplates were used as baffles for CO_2 and light oil molecules.

For the choice of force field, CO_2 was modeled using the EPM2 [69] force field, and the force field for CH_4 was taken from TraPPE-UA [70], while the NERD force field [71] was used for all other alkanes [22]. The nonbonded interactions between atoms were described by the pairwise additive Lennard-Jones 12–6 potentials and the Coulombic interactions.

4.3. Simulation details

In order to be consistent with the conditions of the previous diffusion

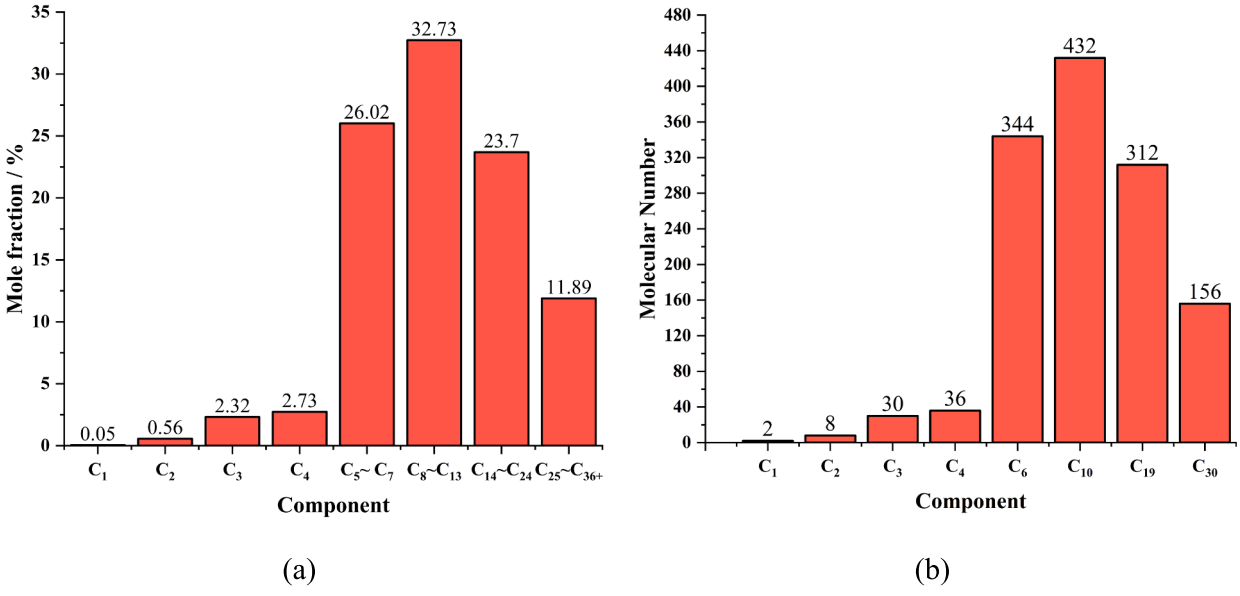

Fig. 6. (a) Chang-7 oil composition, (b) Crude oil model in MD simulations.

experiments, the molecular model of CO_2-light oil system was calculated with constant total volume and temperature. Particularly, the temperature was commanded by Nose-Hoover [72], and the pressure was controlled by applying pressure through He nanoplates. For systems containing CO_2, the particle–particle particle-mesh (PPPM) method was selected to calculate long-range electrostatic interactions with an accuracy of 10^{-5}. Periodic boundary conditions were considered in all simulations, where the cutoff radius was set to 12.0 Å and the time step was set to 1 fs. Notably, all molecular simulations were calculated using the Lammps software package, and the images were rendered using Ovito software.

The simulation process was summarized as follows. Firstly, CO_2 and light oil were needed to reach equilibrium state in the independent He compartments. Then, at 333.15 K, the initial pressure of the CO_2-light oil system was pressurized to 7.5 MPa by applying force to each atom on the He nanoplate at the top and bottom. Subsequently, the He nanoplate in the middle was removed to make CO_2 begin to diffuse into light oil. Meanwhile, the He nanoplates at the top and bottom were fixed to ensure the constant volume of the CO_2-light oil system during the diffusion process. At last, the relevant data in the diffusion process are collected until the end of the simulation.

5. Results and discussion

5.1. Dynamic volume analysis from experiment

5.1.1. Equilibrium pressure and equilibrium time

In all diffusion experiments, the system pressure gradually decreased with time until the dissolution of CO_2 in light oil reached equilibrium. This phenomenon had also been observed through experiments and numerical simulations by Zhou et al. [73], Song et al. [74], and Etminan et al. [75]. With a constant PVT-cell volume, an initial pressure of 7.5 MPa and a constant temperature of 60°C, all measured pressure decay datum was plotted in part a-b of Fig. 7.

From Fig. 7(a) and (b), three obvious sections (rapid diffusion, stable diffusion, and dynamic equilibrium) could be recognized in all the pressure-decay processes [76]. For example, in the case of test #4, the system pressure dropped sharply in the rapid diffusion stage (0–10 min). Then, the pressure dropped gently in the stable diffusion stage (10–45 min). Finally, the pressure signally remained stable with small fluctuations in the dynamic equilibrium stage (45–200 min). Moreover, the duration of the above diffusion stages was closely related to the CO_2-light oil ratio. Comparing test #4 and test #5, the system with relatively low oil content had a relatively short time in the rapid diffusion stage (0–8 min) and stable diffusion stage (8–35 min).

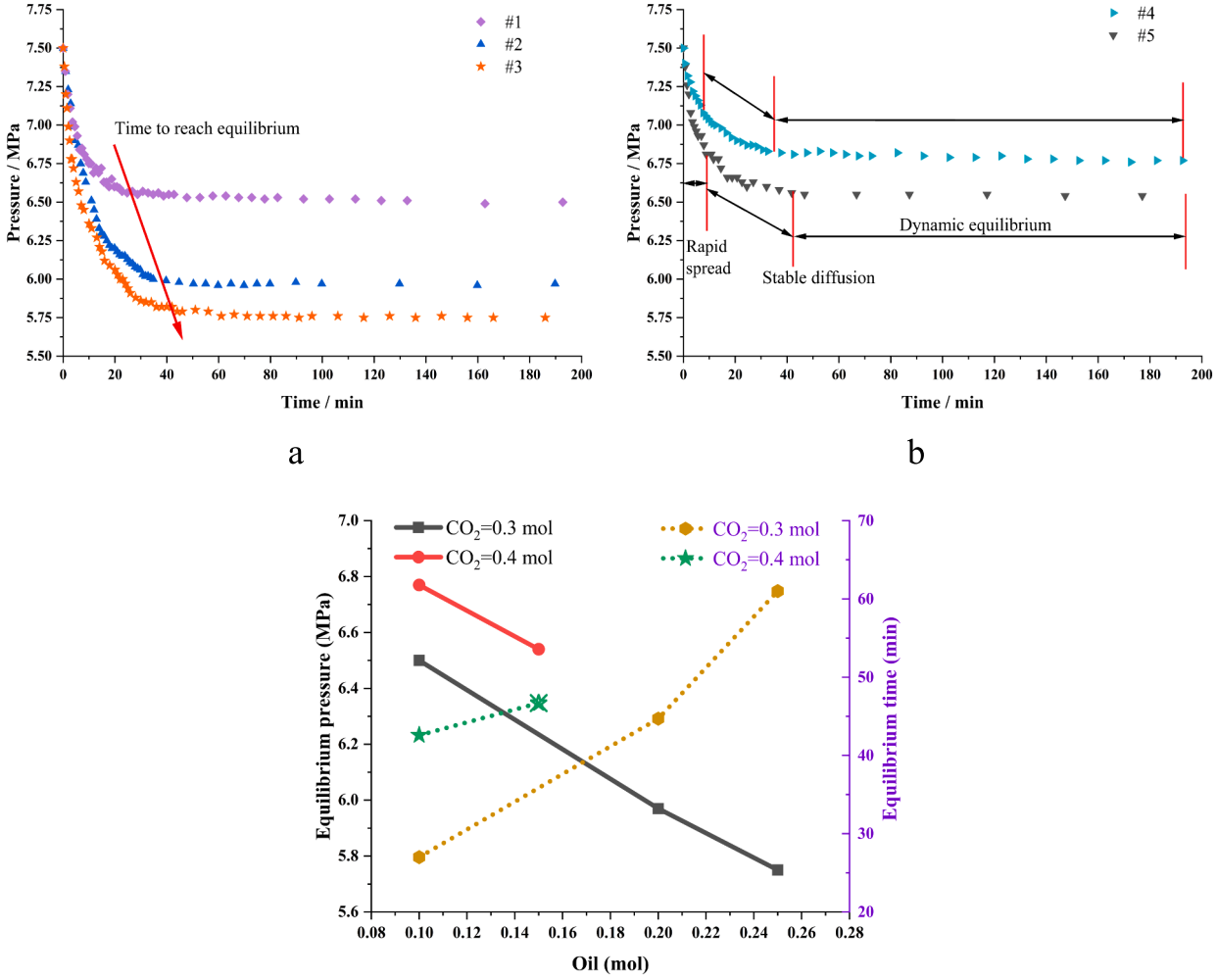

Fig. 7. The relationship between equilibrium pressure and time of CO_2-light oil system: (a) #1, #2 and #3 pressure decay, (b) #4 and #5 pressure decay, (c) Equilibrium time and equilibrium pressure for different CO_2 molar ratios.

According to Fig. 7(c), in all CO_2-light oil systems, when the CO_2 mole number was the same, the light oil mole number was positively proportional to the equilibrium time and inversely proportional to the equilibrium pressure. Contrastively, when the light oil mole number was the same, the relationships between CO_2 mole number, equilibrium time and equilibrium pressure were opposite to the above situation. In conclusion, the larger the volume of light oil phase, the more CO_2 could be dissolved, which led to lower system pressure. However, the light oil near the light oil–gas interface was limited in volume and had tended to be saturated by CO_2, so more time was needed to transfer these CO_2.

5.1.2. CO_2 diffusion coefficient

Diffusion is an essential EOR mechanism for tight unconventional reservoirs, which controls the mixing rate of oil and gas [77]. In gas-oil system, diffusion coefficient is the most intuitive indicator of the speed of diffusion process. Generally, the molecular diffusion coefficient can be measured by direct [46,78] or indirect methods [10,11,36,79–81]. Although the direct method can directly gauge the spatial concentration distribution, it has obvious disadvantages, such as expensive experimental equipment, long laboratory time, and large measurement error. Unlike the direct method, the indirect method is recommended to obtain the diffusion coefficient with simpler experimental procedures and better measurement results. So far, numerous scholars have studied the CO_2 diffusion coefficient in light oil by indirect method. The corresponding research results are presented in Table 4.

The pressure-decay method is a typical indirect method. Via the pressure-decay experiment, the pressure versus time data in CO_2-light oil system was recorded and then fitted to calculate the diffusion coefficient by numerical simulation. As shown in Fig. 8(a-b), the simulation results were fairly consistent with the pressure-decay data under different CO_2-light oil systems. At the constant temperature of 333.15 K and initial pressure of 7.5 MPa, the CO_2 diffusion coefficients in various CO_2-light oil systems were shown in Fig. 8(c). From Fig. 8(c), The diffusion coefficient of CO_2 decreased with the increase of the relative molar ratio of CO_2. The main reason was that when the molar proportion of CO_2 was relatively large, more CO_2 molecules were incorporated into light oil, and the movement space of molecules was relatively small. So, the diffusion coefficient of CO_2 was small.

Notably, the CO_2 diffusion coefficients measured in this paper was larger than that in Table 1 for the following 3 reasons. Firstly, the temperature of this test was relatively high. Usually, the higher temperature leads to higher CO_2 diffusion coefficient in oil phase [81,82], which is mainly due to the increase of kinetic energy of molecules and the decrease of viscosity both in oil and gas phases [26]. Secondly, the pressure in this experiment was much higher than that in Table 1. At the same temperature, the pressure increase of pressure will aggravate the molecular velocity, resulting in the augment of diffusion coefficient [80–82]. Thirdly, the oil used in this paper was light oil, which was easier to be miscible with CO_2 [83–85]. In conclusion, it was reasonable that the CO_2 diffusion coefficient studied in this paper was relatively high.

5.1.3. Swelling factor

In addition to replenishing the formation elastic energy, the oil volume expansion is conducive to turning irreducible oil into movable oil again, thereby increasing oil production. Campos et al. [47] and Lashkarbolooki et al. [48] clarified that the dissolution of CO_2 would cause various degrees of oil volume expansion, which could be characterized by swelling factor. The swelling factor mainly depends on the oil composition and CO_2 content. Normally, this coefficient decreases linearly with the carbon number of alkanes, while increases rapidly with CO_2 content. At present, methods with fixed volume [86,87] or variable volume [88,89] of PVT-cell are primarily selected to survey the oil swelling factor. Table 5 showed the oil swelling factor in different CO_2-light oil systems obtained by these two methods.

In accordance with the previous experiments, the method with fixed PVT-cell volume was adopted to measure the swelling factor in CO_2-light oil system. Fig. 9 provided the comparison of light oil volume at 0 min and 200 min in the previous 5 groups of pressure-decay tests. From the Fig. 9, the light oil volume expansion was more obvious in the system with large oil proportion (#2, #3), while smaller in the system with small oil proportion (#1, #4, #5). Meanwhile, Fig. 10 expressed the comparison of the swelling factors from experiment and simulation, respectively. As shown in the figure, the expansion factor distribution of light oil increased with the increase of the relative molar ratio of CO_2. At the end of the stable diffusion stage, the difference between the fitted values of the experimental values and the simulated values was small, both less than 0.014. The simulated value of the light oil swelling factor was lower than the experimental value. It was because the residual light oil droplets on the inner wall of the PVT bucket at the beginning of CO_2 diffusion are not included in the initial volume (Fig. 9), resulting in a higher coefficient measured by the experimental value. Therefore, the simulated value was used as a reference in MD simulation results. It could be considered that the dynamic swelling factor from simulation could indicate the oil expansion process during the CO_2 diffusion period. Moreover, changing profile of dynamic swelling factor followed synchronous pattern with pressure, which increased rapidly in the rapid diffusion stage, slowly in the stable diffusion stage, and immovably in the dynamic equilibrium stage.

5.1.4. Concentration profile

According to the certain CO_2 diffusion coefficient, the variation of CO_2 concentration in light oil phase with time can be calculated, as shown in Fig. 10(a). In the beginning, CO_2 mostly accumulated on the top of the light oil. Finally, the CO_2 diffusion process was completed at 200 min, where the concentration at the bottom (842.77 mol/m^3) was similar to that at the top (874.30 mol/m^3). Furthermore, there was a significant difference between the CO_2 concentration at the top and bottom as a function of time. The CO_2 concentration at the top gradually transited to the equilibrium concentration, while the CO_2 at the bottom fleetly reached the equilibrium concentration. Hence, in this paper, the second-order decay exponential functions (eq. (26) and eq. (28) were first applied to match the CO_2 concentration curves, and then their derivative functions (eq. (27) and eq. (29) were solved.

Table 4
CO_2 Diffusion coefficient in crude oil/simulated oil.

Author	T/K	P/MPa	Oil sample	M	D/($10^{-8}m^2 \cdot s^{-1}$)
Renner[a] [79]	311.00	1.44 ~ 5.83	Decane	PD	0.73 ~ 1.26
Dong et al. [36]	336.15	2.17	Light oil	PD	1.287
Unatrakarn et al. [80]	303.15 ~ 328.15	2.6 ~ 3.2	Crude oil	PD	1.8 ~ 6.8
Zhang et al. [10]	294.15	3.471	Crude oil	PD	0.48
Tharanivasan et al. [11]	297.05	3.5 ~ 4.2	Heavy oil	PD	0.046 ~ 0.072
Kavousi et al. [81]	295.15 ~ 305.15	1.73 ~ 4.48	Heavy oil	PD	0.036 ~ 0.090
Behzadfar et al. [78]	295.15	2.42 ~ 4.79	Heavy oil	R	0.049 ~ 0.116
Yang et al. [45]	297.05	2.0 ~ 6.0	Heavy oil	HD	0.020 ~ 0.055

Note: D-diffusion coefficient; M−test method; P-test pressure; PD-pressure decay; T-test temperature; R-rheometry; HD-dynamic hanging drop volume analysis [a]-apparent diffusion coefficient in porous media.

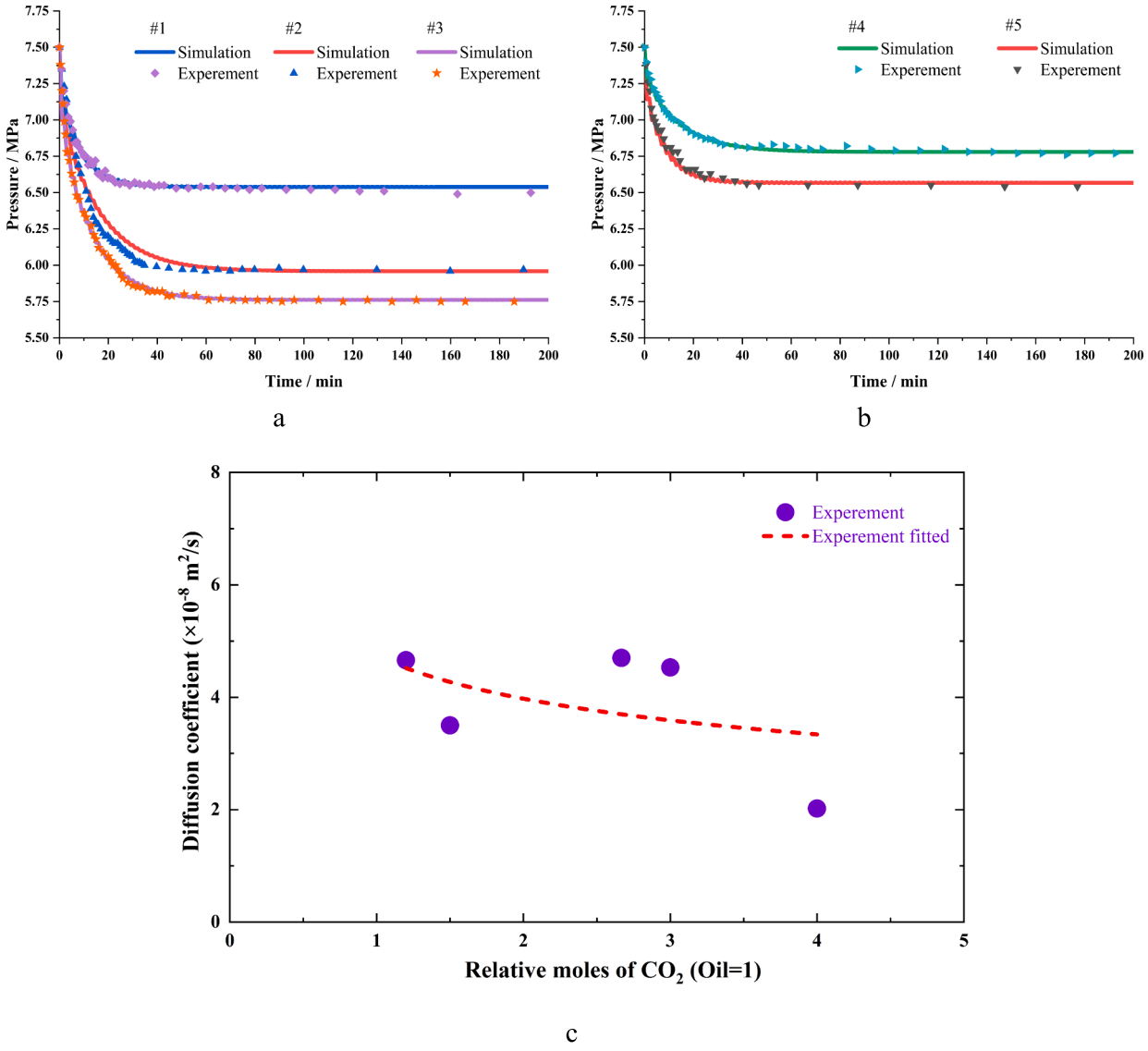

Fig. 8. The pressure decay value of the simulated CO_2 diffusion coefficient via the experiment: (a) #1, #2 and #3 pressure drop value fitting, (b) #4 and #5 pressure drop value fitting, (c) CO_2 diffusion coefficient.

Table 5
Swelling factor of CO_2-crude oil system.

Author	T/K	P/MPa	Oil sample	M	D/($10^{-7}m^2 \cdot s^{-1}$)
Welker et al. [88]	27	0.5 ~ 5.0	Crude oil	FV	1.00 ~ 1.20
Jha et al. [89]	28	3.3 ~ 7.6	Crude oil	FV	1.0580 ~ 1.1564
Li et al. [86]	7 ~ 119	1.0 ~ 41.0	Crude oil	VV	1.0 ~ 1.9
Graue et al. [87]	71	0.7 ~ 10.3	Crude oil	VV	1.00 ~ 1.34

Note: SF-swelling factor; FV- fixed volume; VV- variable volume.

$$C_1(t) = 864.43 + 331.88e^{-\frac{t}{8.48942}} + 472.04e^{-\frac{t}{55.6087}} \quad (38)$$

$$\frac{dC_1(t)}{dt} = -39.0934e^{-\frac{t}{8.48942}} - 8.4886e^{-\frac{t}{55.6087}} \quad (39)$$

$$C_2(t) = 843.60 - 498.56e^{-\frac{t}{9.13075}} - 486.75e^{-\frac{t}{9.13064}} \quad (40)$$

$$\frac{dC_2(t)}{dt} = 54.6023e^{-\frac{t}{9.13075}} + 53.3095e^{-\frac{t}{9.13064}} \quad (41)$$

Fig. 11(a) also plotted the corresponding derivative curves in 0–200 min. According to derivative curves, the decline rate of CO_2 concentration at the top was obviously less than the growth rate at the bottom, which was mainly caused by the dissolution of CO_2 from gas phase to oil phase at the light oil–gas interface. Fig. 11(b) showed the distribution profiles of CO_2 in the light oil system at different times. The gas–liquid interface gradually increased over time due to the gradual dissolution of CO_2 into the light oil system. Thus, the swelling properties of the light oil system were also reflected.

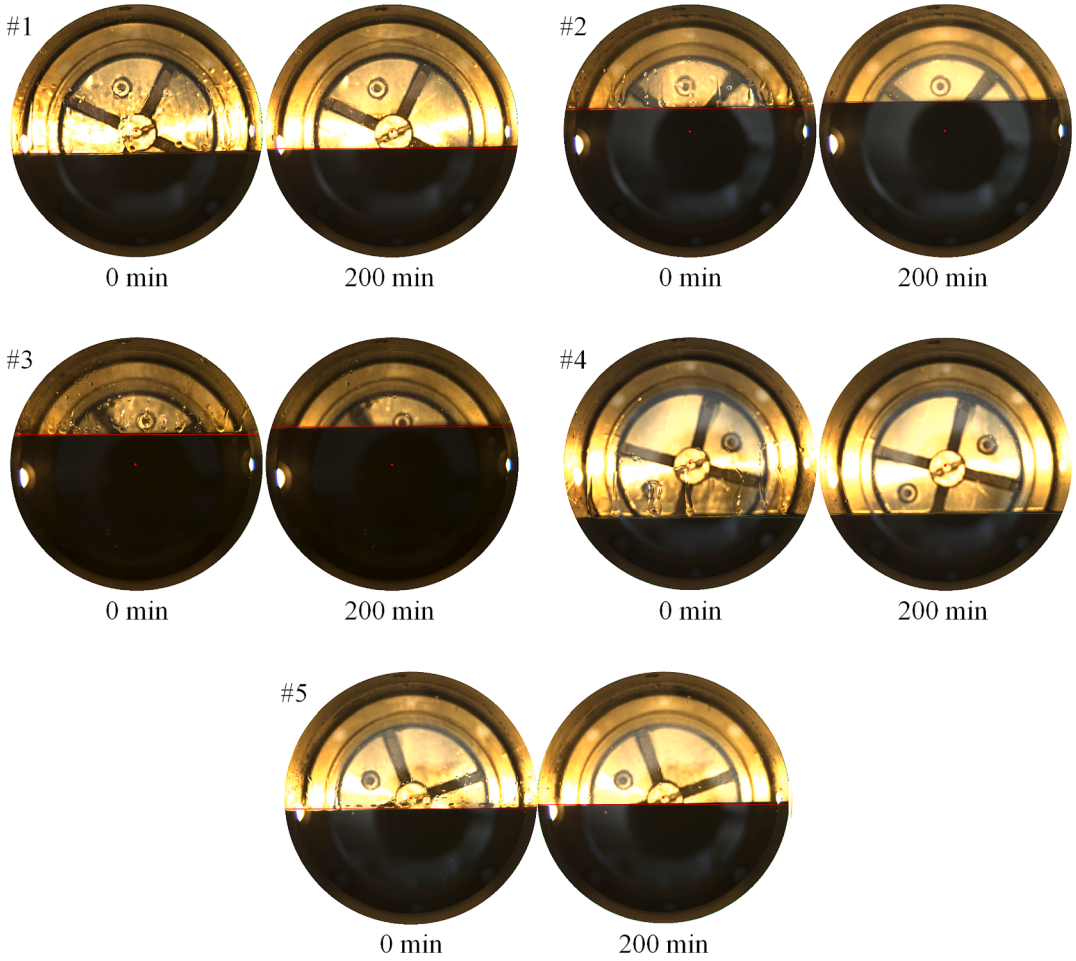

Fig. 9. Cross-sectional view of PVT at different times: #1, #2, #3, #4 and #5.

5.2. Molecular simulation

5.2.1. Density profiles

Fig. 12 showed the entire process from CO_2 equilibrium to diffusion. At the beginning of CO_2 diffusion, it was obvious that the diffusion could be divided into three processes: rapid diffusion, stable diffusion, and dynamic equilibrium. This was consistent with the experimental process. Please refer to the Supplementary material for details of the balancing process. Fig. 13(a) revealed the density distribution of CO_2-light oil system before diffusion process. In the Fig. 13(a), the red curve displayed the light oil density distribution, with an average density of 0.7137 g/cm^3. This density of light oil, which was consisted of various types of molecules, fairly approached the density of real light oil (0.7428 g/cm^3). Similarly, the purple curve showed the CO_2 density distribution, with an average density of 0.1792 g/cm^3. It was only 0.0064 g/cm^3 different from the density (0.1728 g/cm^3) of CO_2 at 333.15 K and 7.5 MPa on the National Institute of Standards and Technology (NIST), indicating that the selection of molecular model of CO_2 was rational. Therefore, the diffusion of CO_2 to light oil could be effectively reflected by the CO_2-light oil molecular system.

Fig. 13(b) expressed the density distribution of light oil (red curve) and CO_2 (purple curve) in the CO_2-light oil system after CO_2 diffusion. From Fig. 13, the light oil average density decreased from 0.7137 g/cm^3 to 0.6701 g/cm^3, where the density of light oil at the intersection of light oil–gas interface dropped obviously. Contrastively, the CO_2 density evenly distributed in the gas phase, peaked at the CO_2-light oil interface, then gradually descended in the light oil phase. CO_2 would accumulate at the CO_2-light oil interface due to the adsorption layer of carbon dioxide molecules at the liquid/gas interface [90,91], which facilitated the diffusion of CO_2 into the Light oil system.

5.2.2. CO_2 diffusion coefficient

This paper calculated the self-diffusion coefficient, MS diffusion coefficient and Fick diffusion coefficient of CO_2.

Fig. 14 showed the self-diffusion coefficient, MS diffusion coefficient, and Fick diffusion coefficient of CO_2 under different CO_2-light oil molar ratios. The self-diffusion coefficient of CO_2 was calculated by the slope of the MSD and time of CO_2 dissolved in light oil. MS diffusion coefficient was calculated by eq. (31), that self-diffusivities were more easily accessible than mutual diffusivities. Combining MS diffusion coefficient with thermodynamic factor, Fick diffusion coefficient was calculated using eq. (37). As seen from the figure, the self-diffusion coefficient and Fick diffusion coefficient gradually decreased with the increase of the molar ratio of CO_2. This is the same as the experimental results. The difference between the fitted values of the experimental values and the simulated values of the CO_2 diffusivity was slight, both less than 1.96×10^{-8} m^2/s. The diffusion coefficient of CO_2 in light oil can be predicted by molecular simulation to a certain extent.

5.2.3. Swelling factor

In previous pressure-decay experiments, the oil swelling factor was defined as the ratio of the saturated oil volume to the initial oil volume [22,92]. At constant mass, the volume is inversely proportional to the density. Thus, the oil swelling factor was characterized by the ratio of oil

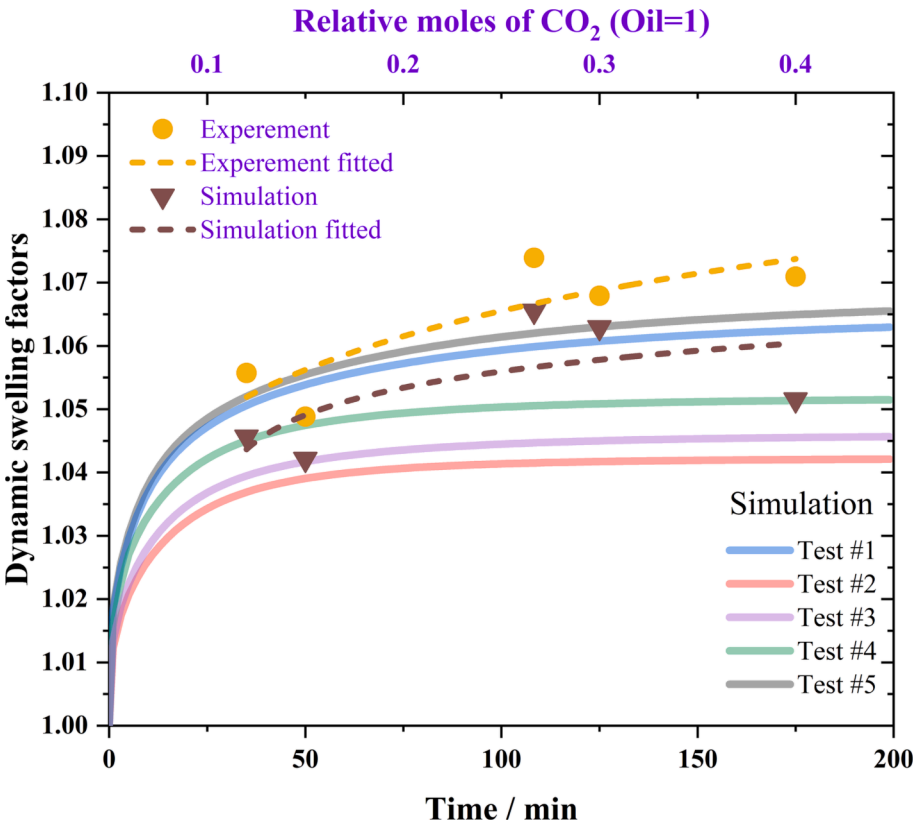

Fig. 10. Profiles of swelling factor: #1, #2, #3, #4 and #5.

density before and after CO_2 diffusion process.

Fig. 15 showed the comparison between the light oil swelling factor calculated from the average density of oil before CO_2 diffusion (6 ns) and that after CO_2 diffusion (18 ns), the experimental and simulated values. According to the figure, the swelling factor of light oil gradually increased with the increase of the relative molar ratio of CO_2. The error between the fitted value of the swelling factor calculated by MD and that calculated by Dynamic Volume Analysis (DVA) was relatively small, and the difference was less than 0.006. The results of MD calculation can predict the swelling factor of light oil well and can be used to predict the swelling factor of crude oil.

5.2.4. Oil Self-diffusion coefficient and potential energy

The potential energy can reflect the stability of the substance. The lower the potential energy, the more stable the state of the substance. For the potential energy calculation, we used the conventional potential energy calculation method. The total potential energy of the system as a function of the N atom coordinates:

$$E(r_1, r_2, \cdots, r_N) = \sum_{i,j} E_{pair}(r_i, r_j) + \sum_{i,j} E_{bond}(r_i, r_j) + \sum_{i,j} E_{angle}(r_i, r_j, r_k) + \sum_{i,j} E_{dihedral}(r_i, r_j, r_k, r_l)$$

where the first term is the sum of all non-bonded pairwise interactions, including long-range Coulombic interactions, the second through fifth terms are bond, angle, and dihedral, respectively.

In this paper, the potential energy of the light oil system after CO_2 diffusion was calculated by layers (Fig. 16), where the thickness of each layer was 2 nm. From the Fig. 16, Z = 20 nm was approximately the interface between CO_2 and light oil. Using median value to represent the average atomic potential energy of each light oil layer. The average atomic potential energy variation characteristics were conformed to the Poisson distribution within 16.0–18.0 ns. Moreover, the potential energy was the largest in the vicinity of the interface (18–20 nm) and gradually decreased as it moved away from the CO_2 interface. The average atomic potential energy was positively correlated with the amount of dissolved CO_2. This shows that the greater the amount of CO_2 dissolved in the crude oil during the process of CO_2 flooding, the more unstable the crude oil is, and the easier the crude oil is to be extracted. This was conducive to improving CO_2 EOR. In addition, the light oil self-diffusion coefficient of each layer could also reflect the oil stability. It could be seen that the self-diffusion coefficient of the light oil closer to the interface was larger, indicating that the movement of the light oil was stronger in the interface region.

6. Conclusion

This paper selected the light oil of Chang 7 in the Ordos Basin as the research object. The physical simulation experiment of CO_2-light oil two-phase system diffusion was conducted by PVT. Based on Fick's second law of diffusion, PR EOS and material balance method, the CO_2 diffusion process in light oil system was described. The diffusion behavior of CO_2 in light oil and the expansion behavior of light oil were studied. In addition, the behavior of mass transfer between CO_2 and light oil was also studied by molecular dynamics simulation method to verify the results from above-mentioned experiments. The main conclusions were as follows:

1. The pressure decay process of CO_2-light oil was fitted by the revised equation calculation. Specially, the equilibrium period of pressure decay process was emphatically matched, which was different from studies of previous scholars. Furthermore, the equilibrium pressure and equilibrium time of the system were related to the ratio of CO_2-light oil.

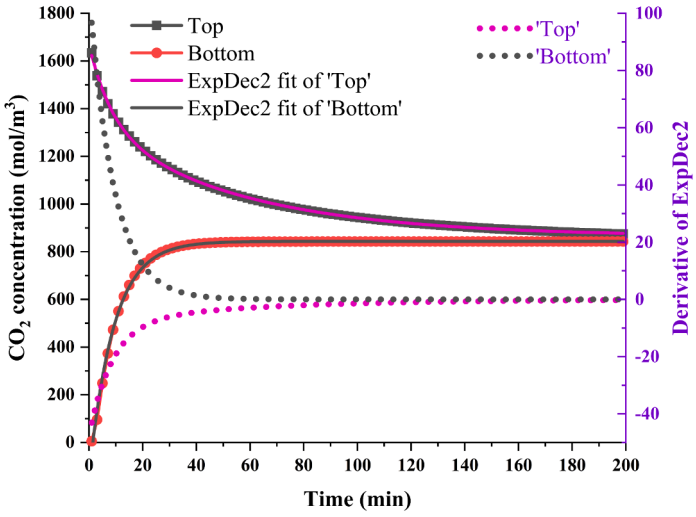

(a)

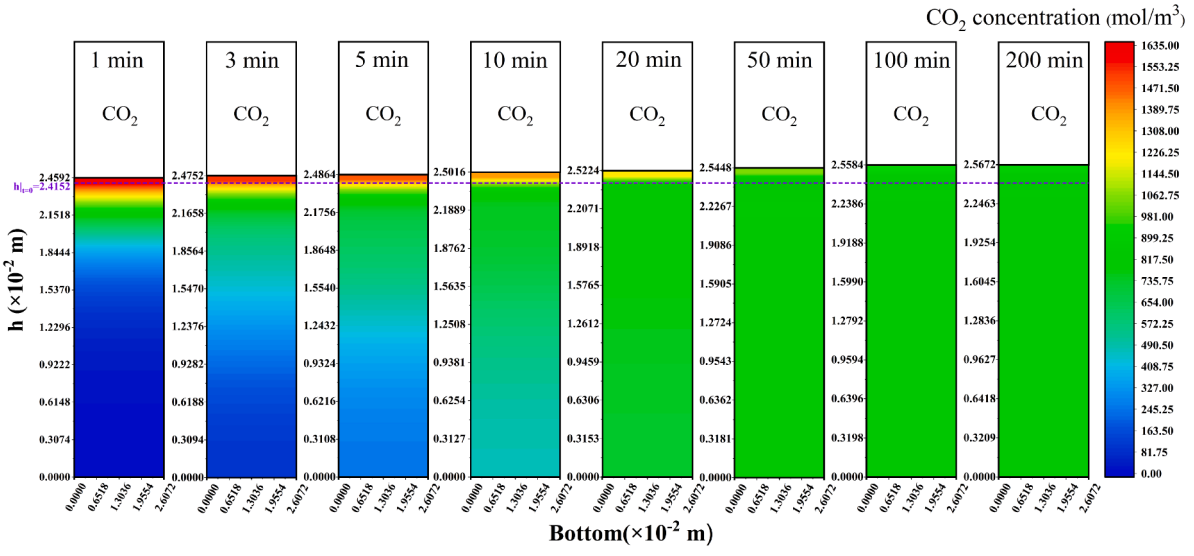

(b)

Fig. 11. Profiles of CO_2 concentration: (a) Fitted curves of CO_2 concentrations at the top and bottom of the crude oil, (b) The interfacial height of crude oil, and the CO_2 concentration distribution at different times.

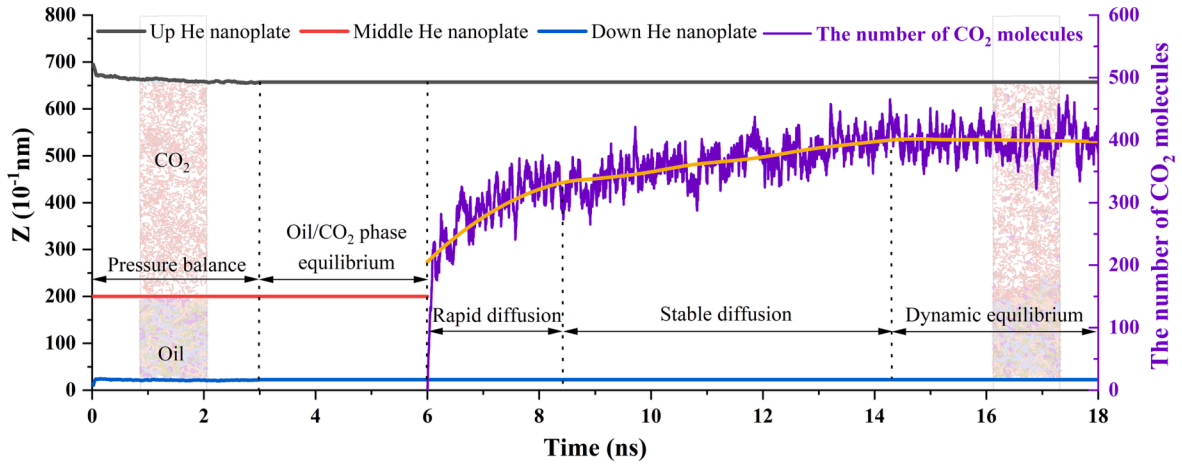

Fig. 12. Molecular distribution of CO_2 at different times.

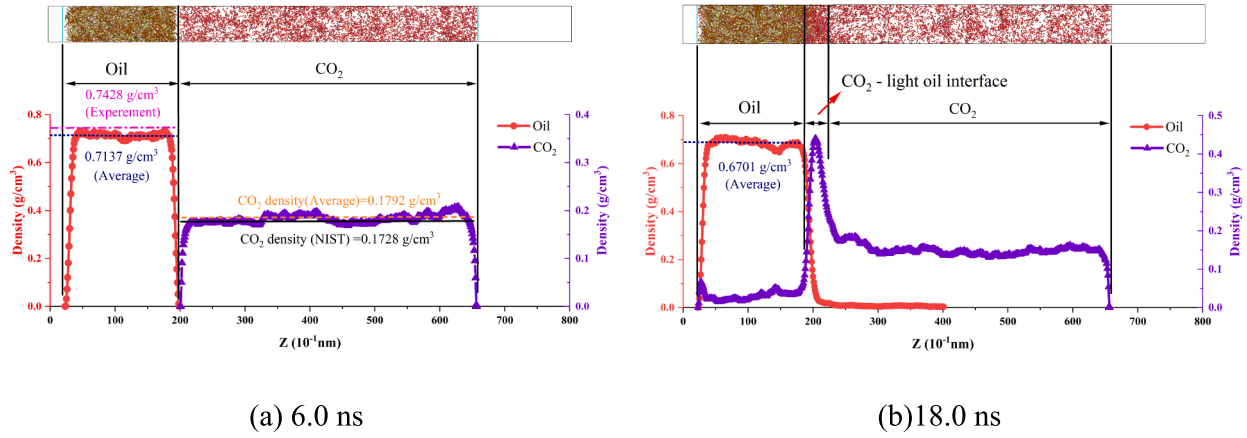

Fig. 13. Density distribution of CO_2 and light oil: (a) 6.0 ns, (b) 18.0 ns.

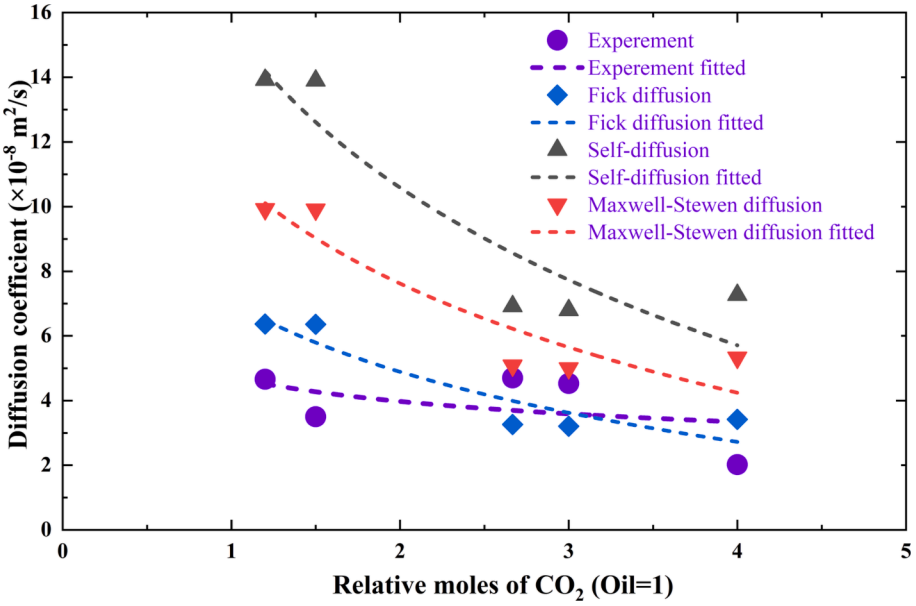

Fig. 14. Comparison of CO_2 diffusion coefficients between MD and experiment.

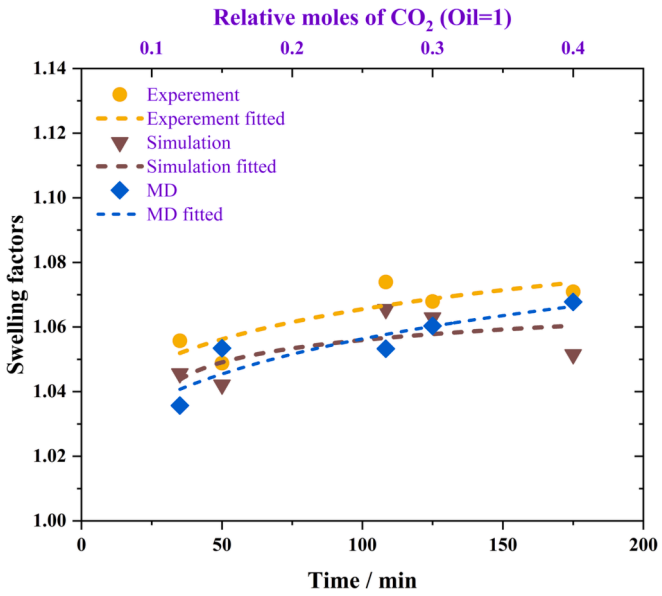

Fig. 15. Comparison of light oil swelling factor between MD and experiment.

2. The CO_2 concentration distribution and the dynamic expansion factor of light oil were consistent with the pressure decay process. Generally, the change rate was relatively fast in the initial stage, and then gradually tended to balance.
3. Synthetically, the results from experiment, numerical simulation and molecular dynamics simulation were fairly verified with each other. Under the condition of temperature of 333.15 K and initial pressure of 7.5 MPa, the diffusion coefficient of CO_2 decreased with the increase of the relative molar ratio of CO_2, the difference between the fitted values of the experimental values and the simulated values of the CO_2 diffusivity was small, both less than 1.96×10^{-8} m2/s. The swelling factor of light oil gradually increased with the increase of the relative molar ratio of CO_2. The error between the fitted value of the swelling factor calculated by MD and that calculated by Dynamic Volume Analysis was relatively small, and the difference was less than 0.006. Therefore, the CO_2 Fick diffusion coefficient in light oil can be obtained from the more readily available self-diffusion coefficient.
4. CO_2 would aggregate at the CO_2-light oil interface, and the density of CO_2 would have a peak at the CO_2-light oil interface, which increased the mass transfer rate between CO_2 and light oil at the interface. Therefore, in light oil phase, the change rate of CO_2 concentration at the interface was faster than that at the bottom.
5. After CO_2 is dissolved in light oil, the closer to the CO_2-light oil interface, the greater the potential energy and self-diffusion coefficient of the light oil. It shows that CO_2 can increase the mobility of light oil.

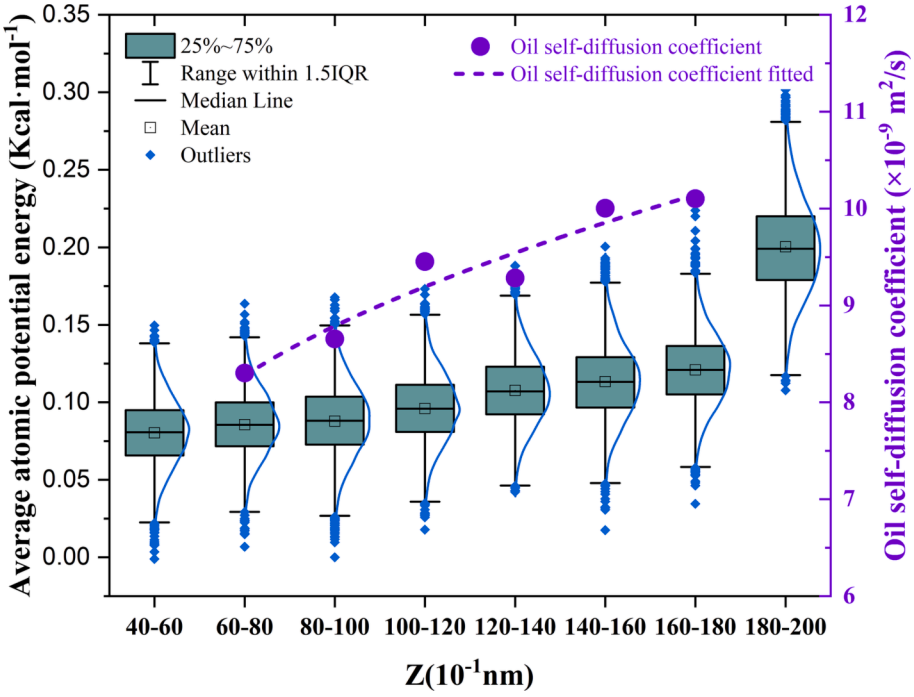

Fig. 16. Average atomic potential energy and self-diffusion coefficient of light oil at different positions.

CRediT authorship contribution statement

Yongcheng Luo: Conceptualization, Writing – original draft, Investigation, Methodology, Data curation, Formal analysis, Visualization. **Hanmin Xiao:** Resources, Funding acquisition, Supervision. **Xiangui Liu:** Project administration. **Taiyi Zheng:** Writing – review & editing, Validation, Investigation. **Zhenkai Wu:** Writing – review & editing.

Declaration of Competing Interest

The authors declare that they have no known competing financial interests or personal relationships that could have appeared to influence the work reported in this paper.

Data availability

I have shared the Supplementary Material at the Attach Files step

Acknowledgements

This work was supported by the CNPC basic advanced reserve technology (2021DJ2201).

Appendix A. Supplementary data

Supplementary data to this article can be found online at https://doi.org/10.1016/j.molliq.2023.121943.

References

[1] Z. Song, Y. Song, Y. Li, B. Bai, K. Song, J. Hou, A critical review of CO_2 enhanced oil recovery in tight oil reservoirs of North America and China, Fuel 276 (2020) 118006, https://doi.org/10.1016/j.fuel.2020.118006.
[2] X. Tang, Y. Li, X. Han, Y. Zhou, J. Zhan, M. Xu, R. Zhou, K. Cai, X. Chen, L. Wang, Dynamic characteristics and influencing factors of CO_2 huff and puff in tight oil reservoirs, Pet. Explor. Dev. 48 (2021) 946–955, https://doi.org/10.1016/S1876-3804(21)60079-4.
[3] Y. Zhang, W. Guo, Molecular insight into the tight oil movability in nano-pore throat systems, Fuel 293 (2021) 120428, https://doi.org/10.1016/j.fuel.2021.120428.
[4] B. Wei, X. Zhang, J. Liu, X. Xu, W. Pu, M. Bai, Adsorptive behaviors of supercritical CO_2 in tight porous media and triggered chemical reactions with rock minerals during CO_2-EOR and -sequestration, Chem. Eng. J. 381 (2020) 122577, https://doi.org/10.1016/j.cej.2019.122577.
[5] L. Wang, Y. He, Q. Wang, M. Liu, X. Jin, Multiphase flow characteristics and EOR mechanism of immiscible CO_2 water-alternating-gas injection after continuous CO_2 injection: a micro-scale visual investigation, Fuel 282 (2020) 118689, https://doi.org/10.1016/j.fuel.2020.118689.
[6] L. Fan, L. Li, Y. Su, M. Cai, M. Tang, X. Gao, Z. Chen, C. Wang, CO_2-prepad injection EOR simulation and sensitivity analysis considering miscibility and geomechanics in tight oil reservoirs, J. Pet. Sci. Eng. 195 (2020) 107905, https://doi.org/10.1016/j.petrol.2020.107905.
[7] X. Huang, X. Li, Y. Zhang, T. Li, R. Zhang, Microscopic production characteristics of crude oil in nano-pores of shale oil reservoirs during CO_2 huff and puff, Pet. Explor. Dev. 49 (2022) 636–643, https://doi.org/10.1016/S1876-3804(22)60053-3.
[8] M. Zuo, H. Chen, X. Qi, X. Liu, C. Xu, H. Yu, M.S. Brahim, Y. Wu, H. Liu, Effects of CO_2 injection volume and formation of in-situ new phase on oil phase behavior during CO_2 injection for enhanced oil recovery (EOR) in tight oil reservoirs, Chem. Eng. J. 452 (2023) 139454, https://doi.org/10.1016/j.cej.2022.139454.
[9] M.R. Riazi, A new method for experimental measurement of diffusion coefficients in reservoir fluids, J. Petrol. Sci. Eng. 14 (1996) 235–250, https://doi.org/10.1016/0920-4105(95)00035-6.
[10] Y.P. Zhang, C.L. Hyndman, B.B. Maini, Measurement of gas diffusivity in heavy oils, J. Pet. Sci. Eng. 25 (2000) 37–47, https://doi.org/10.1016/S0920-4105(99)00031-5.
[11] A.K. Tharanivasan, C. Yang, Y. Gu, Measurements of molecular diffusion coefficients of carbon dioxide, methane, and propane in heavy oil under reservoir conditions, Energy Fuels 20 (2006) 2509–2517, https://doi.org/10.1021/ef060080d.
[12] P. Guo, Z. Wang, P. Shen, J. Du, Molecular diffusion coefficients of the multicomponent gas-crude oil systems under high temperature and pressure, Ind. Eng. Chem. Res. 48 (2009) 9023–9027, https://doi.org/10.1021/ie801671u.
[13] H. Ahmadi, M. Jamialahmadi, B.S. Soulgani, N. Dinarvand, M.S. Sharafi, Experimental study and modelling on diffusion coefficient of CO_2 in water, Fluid Phase Equilib. 523 (2020) 112584, https://doi.org/10.1016/j.fluid.2020.112584.
[14] H. Sun, H. Li, D. Yang, Coupling heat and mass transfer for a gas mixture–heavy oil system at high pressures and elevated temperatures, Int. J. Heat Mass Transf. 74 (2014) 173–184, https://doi.org/10.1016/j.ijheatmasstransfer.2014.03.004.
[15] W. Liu, L. Du, X. Qin, X. Chen, W. Liu, X. Luo, Numerical modeling of CO_2 diffusion into water-oil liquid system using moving mesh technique, Fuel 261 (2020) 116426, https://doi.org/10.1016/j.fuel.2019.116426.
[16] B. Liu, J. Shi, B. Sun, Y. Shen, J. Zhang, X. Chen, M. Wang, Molecular dynamics simulation on volume swelling of CO_2-alkane system, Fuel 143 (2015) 194–201, https://doi.org/10.1016/j.fuel.2014.11.046.
[17] M. Mehana, M. Fahes, L. Huang, System Density of Oil-Gas Mixtures: Insights from Molecular Simulations, SPE 2017 187297, 10.2118/187297-MS.
[18] C. Li, H. Pu, J.X. Zhao, Molecular simulation study on the volume swelling and the viscosity reduction of n-alkane/CO_2 systems, Ind. Eng. Chem. Res. 58 (2019) 8871–8877, https://doi.org/10.1021/acs.iecr.9b01268.
[19] P. Zhang, Y. Ji, W. Li, L. Xu, L. Wang, D. Fu, Investigation of viscosity, activation energy and CO2 diffusion coefficient for N-methyl-1,3-propane-diamine, N-(2-aminoethyl)ethanolamine and 1,4-butanediamine activated 2-diethylaminoethanol aqueous solutions, J. Chem. Thermodyn. 168 (2022) 106740, https://doi.org/10.1016/j.jct.2022.106740.
[20] S. Omrani, M. Ghasemi, S. Mahmoodpour, A. Shafiei, B. Rostami, Insights from molecular dynamics on CO2 diffusion coefficient in saline water over a wide range of temperatures, pressures, and salinity: CO2 geological storage implications, J. Mol. Liq. 345 (2022) 117868, https://doi.org/10.1016/j.molliq.2021.117868.
[21] X. Zhao, H. Jin, Y. Chen, Z. Ge, Numerical study of H_2, CH_4, CO, O_2 and CO_2 diffusion in water near the critical point with molecular dynamics simulation, Comput. Math. Appl. 81 (2021) 759–771, https://doi.org/10.1016/j.camwa.2019.11.012.
[22] C. Li, H. Pu, X. Zhong, Y. Li, J.X. Zhao, Interfacial interactions between Bakken crude oil and injected gases at reservoir temperature: a molecular dynamics simulation study, Fuel 276 (2020) 118058, https://doi.org/10.1016/j.fuel.2020.118058.
[23] X. Huang, Y. Zhang, M. He, X. Lia, W. Yang, J. Lu, Asphaltene precipitation and reservoir damage characteristics of CO_2 flooding in different microscopic structure types in tight oil reservoirs, Fuel 312 (2022) 122943, https://doi.org/10.1016/j.fuel.2021.122943.
[24] W. Dang, H. Nie, J. Zhang, X. Tang, S. Jiang, X. Wei, Y. Liu, F. Wang, P. Li, Z. Chen, Pore-scale mechanisms and characterization of light oil storage in shale nanopores: new method and insights, Geosci. Front. 13 (2022) 101424, https://doi.org/10.1016/j.gsf.2022.101424.
[25] S. Jiang, L. Chen, Y. Wu, Z. Jiang, E. McKenna, Hybrid plays of upper triassic Chang7 lacustrine source rock interval of Yanchang Formation, Ordos Basin, China, J. Pet. Sci. Eng. 159 (2017) 182–196, https://doi.org/10.1016/j.petrol.2017.09.033.
[26] S. Zheng, D. Yang, Determination of individual diffusion coefficients of C3H8/n-C4H10/CO_2/heavy oil systems at high pressures and elevated temperatures by dynamic volume analysis (DVA), SPE J. 22 (2017) 799–816, https://doi.org/10.2118/179618-PA.
[27] M.R. Yassin, A. Habibi, A. Zolfaghari, S. Eghbali, H. Dehghanpour, An experimental study of nonequilibrium carbon dioxide/oil interactions, SPE J. 23 (2018) 1768–1783, https://doi.org/10.2118/187093-PA.
[28] M. Jamialahmadi, M. Emadi, H. Müller-Steinhagen, Diffusion coefficients of methane in liquid hydrocarbons at high pressure and temperature, J. Petrol. Sci. Eng. 53 (2006) 47–60, https://doi.org/10.1016/j.petrol.2006.01.011.
[29] A.K. Tharanivasan, C. Yang, Y. Gu, Comparison of three different interface mass transfer models used in the experimental measurement of solvent diffusivity in heavy oil, J. Petrol. Sci. Eng. 44 (2004) 269–282, https://doi.org/10.1016/j.petrol.2004.03.003.
[30] B.I. Lee, M.G. Kesler, A Generalized thermodynamic correlation based on three-parameter corresponding states, AIChE J. 21 (1975) 510–527, https://doi.org/10.1002/aic.690210313.
[31] S.B. Hawthorne, D.J. Miller, L. Jin, C.D. Gorecki, Rapid and simple capillary-rise/vanishing interfacial tension method to determine crude oil minimum miscibility pressure: pure and mixed CO_2, methane, and ethane, Energy Fuels 30 (2016) 6365–6372, https://doi.org/10.1021/acs.energyfuels.6b01151.
[32] P.L. Chueh, J.M. Prausnitz, Vapor–liquid equilibria at high pressures: calculation of partial molar volumes in nonpolar liquid mixtures, AIChE J. 13 (1967) 1099–1107, https://doi.org/10.1002/aic.690130612.
[33] S. Zheng, H. Li, H. Sun, D. Yang, Determination of diffusion coefficient for alkane solvent–CO_2 mixtures in heavy oil with consideration of swelling effect, Ind. Eng. Chem. Res. 55 (2016) 1533–1549, https://doi.org/10.1021/acs.iecr.5b03929.
[34] S. Zheng, H. Sun, D. Yang, Coupling heat and mass transfer for determining individual diffusion coefficient of a hot C3H8–CO_2 mixture in heavy oil under reservoir conditions, Int. J. Heat Mass Transf. 102 (2016) 251–263, https://doi.org/10.1016/j.ijheatmasstransfer.2016.05.136.
[35] H. Li, D. Yang, Determination of individual diffusion coefficients of solvent/CO_2 mixture in heavy oil with pressure-decay method, SPE J. 21 (2016) 131–143, https://doi.org/10.2118/176032-PA.
[36] X. Dong, Y. Shi, D. Yang, Quantification of mutual mass transfer of CO_2/N2−light oil systems by dynamic volume analysis, Ind. Eng. Chem. Res. 57 (2018) 16495–16507, https://doi.org/10.1021/acs.iecr.8b03983.
[37] D. Peng, D.B. Robinson, A new two-constant equation of state, Ind. Eng. Chem. Fundam. 15 (1976) 59–64, https://doi.org/10.1021/i160057a011.
[38] A. Péneloux, E. Rauzy, R. Freze, A consistent correction for Redlich–Kwong–Soave volumes, Fluid Phase Equilib. 8 (1982) 7–23, https://doi.org/10.1016/0378-3812(82)80002-2.

[39] H. Li, D. Yang, Modified a function for the Peng-Robinson equation of state to improve the vapor pressure prediction of non-hydrocarbon and hydrocarbon compounds, Energy Fuels 25 (2011) 215–223, https://doi.org/10.1021/ef1009272.

[40] Y. Shi, X. Li, D. Yang, Nonequilibrium phase behaviour of alkane solvent(s)–CO_2–heavy oil systems under reservoir conditions, Ind. Eng. Chem. Res. 55 (2016) 2860–2871, https://doi.org/10.1021/acs.iecr.5b04831.

[41] X. Li, H. Li, D. Yang, Determination of multiphase boundaries and swelling factors of solvent(s)–CO_2–heavy oil systems at high pressures and elevated temperatures, Energy Fuels 27 (2013) 1293–1306, https://doi.org/10.1021/ef301866e.

[42] X. Sun, L. Cai, Z. Song, Y. Zhang, Y. Shi, A novel model for determination of apparent diffusion coefficient of gaseous solvent mixture-heavy oil system with consideration of swelling effect and density variation, Fluid Phase Equilib. 549 (2021) 113207, https://doi.org/10.1016/j.fluid.2021.113207.

[43] M. Hafez, A.P. Ratanpara, Y. Martiniere, M. Dagois, M. Ghazvini, M. Kavosi, P. Mandin, M. Kim, CO2-monoethanolamine-induced oil swelling and viscosity reduction for enhanced oil recovery, J. Petrol. Sci. Eng. 206 (2021) 109022, https://doi.org/10.1016/j.petrol.2021.109022.

[44] S. Fakher, A. Imqam, An experimental investigation of immiscible carbon dioxide interactions with crude oil: oil swelling and asphaltene agitation, Fuel 269 (2020) 117380, https://doi.org/10.1016/j.fuel.2020.117380.

[45] C. Yang, Y. Gu, Diffusion coefficients and oil swelling factors of carbon dioxide, methane, ethane, propane, and their mixtures in heavy oil, Fluid Phase Equilib. 243 (2006) 64–73, https://doi.org/10.1016/j.fluid.2006.02.020.

[46] X. Li, D. Yang, Z. Fan, Vapor-liquid phase boundaries and swelling factors of C3H8-n-C4H10-CO_2-heavy oil systems under reservoir conditions, Fluid Phase Equilib. 434 (2017) 211–221, https://doi.org/10.1016/j.fluid.2016.12.004.

[47] C.E.P.S. Campos, H.G.D. Villardi, F.L.P. Pessoa, A.M.C. Uller, Solubility of carbon dioxide in water and hexadecane: experimental measurement and thermodynamic modeling, J. Chem. Eng. Data 54 (2009) 2881–2886, https://doi.org/10.1021/je800966f.

[48] M. Lashkarbolooki, A. Vaezian, A.Z. Hezave, S. Ayatollahi, M. Riazi, Experimental investigation of the influence of supercritical carbon dioxide and supercritical nitrogen injection on tertiary live-oil recovery, J. Supercrit. Fluids 117 (2016) 260–269, https://doi.org/10.1016/j.supflu.2016.07.004.

[49] R. Simon, D.J. Graue, Generalized correlations for predicting solubility, swelling and viscosity behavior of CO_2 -crude oil systems, J. Pet. Technol. 17 (1965) 102–106, https://doi.org/10.2118/917-PA.

[50] C.F. Spencer, R.P. Danner, Prediction of bubble point density of mixtures, J. Chem. Eng. Data 18 (1973) 230–233, https://doi.org/10.1021/je60057a007.

[51] R.C. Eberhart, J. Kennedy, A new optimizer using particle swarm theory, Proceedings of the Sixth International Symposium on Micro Machine and Human Science 1 (1995) (1995) 39–43, https://doi.org/10.1109/MHS.1995.494215.

[52] N. Alharthy, T. Teklu, H. Kazemi, R. Graves, S. Hawthorne, J. Braunberger, B. Kurtoglu, Enhanced oil recovery in liquid-rich shale reservoirs: laboratory to field, Soc. Petrol. Eng. (2015), https://doi.org/10.2118/175034-MS.

[53] G.E. Archie, The electrical resistivity log as an aid in determining some reservoir characteristics, Petroleum Technology (January 1942).

[54] F. Lyu, Z. Ning, S. Yang, Z. Mu, Z. Cheng, Z. Wang, B. Liu, Molecular insights into supercritical methane sorption and self-diffusion in monospecific and composite nanopores of deep shale, J. Mol. Liq. 359 (2022) 119263, https://doi.org/10.1016/j.molliq.2022.119263.

[55] Y. Xia, S. Wei, Y. Jin, K. Chen, Self-diffusion flow and heat coupling model applicable to the production simulation and prediction of deep shale gas wells, Nat. Gas Ind. B 8 (2021) 359–366, https://doi.org/10.1016/j.ngib.2021.07.006.

[56] X. Cao, M. Zhou, Shengkun Jiaa, Xigang Yuanabc, Yu Kuo-Tsong, Maxwell-Stefan diffusion coefficient model derived from entropy generation minimization principle for binary liquid mixtures, Chem. Eng. Sci. 207 (2) (November 2019) 30–38, https://doi.org/10.1016/j.ces.2019.06.011.

[57] A. Kubaczka, W. Kamiński, J. Marszałek, Predicting mass fluxes in the pervaporation process using Maxwell-Stefan diffusion coefficients, J. Membr. Sci. 546 (2018) 111–119, https://doi.org/10.1016/j.memsci.2017.08.074.

[58] Thiago J.P. dos Santos, Frederico W. Tavares, Charlles R.A. Abreu, Fick diffusion coefficients via molecular dynamics: an alternative approach in the Fourier domain, J. Mol. Liquids 329 (2021) 115460, https://doi.org/10.1016/j.molliq.2021.115460.

[59] X. Zhao, T. Luo, H. Jin, A predictive model for self-, Maxwell-Stefan, and Fick diffusion coefficients of binary supercritical water mixtures, J. Mol. Liq. 324 (2021) 114735, https://doi.org/10.1016/j.molliq.2020.114735.

[60] Y. Zhao, Y. Feng, X. Zhang, Molecular simulation of CO2/CH4 self- and transport diffusion coefficients in coal, Fuel 165 (2016) 19–27, https://doi.org/10.1016/j.fuel.2015.10.035.

[61] R. Krishna, J.M. van Baten, The darken relation for multicomponent diffusion in liquid mixtures of linear alkanes: an investigation using molecular dynamics (MD) simulations, Ind. Eng. Chem. Res. 44 (2005) 6939–6947, https://doi.org/10.1021/ie050146c.

[62] X. Zhao, H. Jin, Correlation for self-diffusion coefficients of H2, CH4, CO, O2 and CO2 in supercritical water from molecular dynamics simulation, Appl. Therm. Eng. 171 (2020) 114941, https://doi.org/10.1016/j.applthermaleng.2020.114941.

[63] H. Long, H. Lin, M. Yan, Y. Bai, X. Tong, X. Kong, S. Li, Adsorption and diffusion characteristics of CH4, CO2, and N2 in micropores and mesopores of bituminous coal: molecular dynamics, Fuel 292 (2021) 120268, https://doi.org/10.1016/j.fuel.2021.120268.

[64] L.S. Darken, Trans. Am. Inst. Min. Metall. Eng. 175 (1948) 184.

[65] X. Liu, Sondre K. Schnell, Jean-Marc Simon, Peter Krüger, Dick Bedeaux, Signe Kjelstrup, André Bardow, Thijs J.H. Vlugt, Diffusion coefficients from molecular dynamics simulations in binary and ternary mixtures, Int. J. Thermophys. 34 (2013) 1169–1196, https://doi.org/10.1007/s10765-013-1482-3.

[66] A. Vignes, Predictive Theory for Multicomponent Diffusion Coefficients, Ind. Eng. Chem. Fundamen. 6 (1967) 614–616, https://doi.org/10.1021/i160024a022.

[67] B. Smit, T.L.M. Maesen, Molecular simulations of zeolites: adsorption, diffusion, and shape selectivity, Chem. Rev. 108 (10) (2008) 4125–4184.

[68] F. Peng, R. Wang, Z. Guo, G. Feng, Molecular dynamics simulation to estimate minimum miscibility pressure for oil with pure and impure CO2, J. Phys. Commun. 2 (2018) 115028, https://doi.org/10.1088/2399-6528/aaf090.

[69] J.G. Harris, K.H. Yung, Carbon Dioxide's liquid-vapor coexistence curve and critical properties as predicted by a simple molecular model, J. Phys. Chem. 99 (1995) 12021–12024, https://doi.org/10.1021/j100031a034.

[70] M.G. Martin, J.I. Siepmann, Transferable potentials for phase equilibria. 1. unitedatom description of n-alkanes, J. Phys. Chem. B 102 (1998) 2569–2577, https://doi.org/10.1021/jp990822m.

[71] S.K. Nath, F.A. Escobedo, J.J. De Pablo, On the simulation of vapor-liquid equilibria for alkanes, J. Chem. Phys. 108 (1998) 9905–9911, https://doi.org/10.1063/1.476429.

[72] X. Li, S. Wang, Q. Feng, Q. Xue, The miscible behaviors of C10H22(C7H17N)/C3H8 system: Insights from molecular dynamics simulations, Fuel 279 (2020) 118445, https://doi.org/10.1016/j.fuel.2020.118445.

[73] X. Zhou, Q. Jiang, Q. Yuan, L. Zhang, J. Feng, B. Chu, F. Zeng, G. Zhu, Determining CO2 diffusion coefficient in heavy oil in bulk phase and in porous media using experimental and mathematical modeling methods, Fuel 263 (2020) 116205, https://doi.org/10.1016/j.fuel.2019.116205.

[74] Song L, Kantzas A, Bryan J, Experimental measurement of diffusion coefficient of CO2 in heavy oil using X-ray computed-assisted tomography under reservoir conditions, in: Can. Unconv. Resour. Int. Pet. Conf., Calgary, Alberta, Canada, 2010. 10.2118/137545-MS.

[75] S.R. Etminan, B.B. Maini, Z.H. Chen, Hassanzadeh, Constant-pressure technique for gas diffusivity and solubility measurements in heavy oil and bitumen, Energy Fuels 24 (2010) 533–549, https://doi.org/10.1021/ef9008955.

[76] T. Zheng, Y. Luo, Y. Shi, X. Liu, Z. Yang, Y. Luo, Y. Zhang, The Effects of Gas Mixture Composition on the Mass Transfer and Individual Diffusion Coefficient in CH4-CO2-Light Oil Systems, ASME 2021 40th International Conference on Ocean, Offshore and Arctic Engineering 2021 10.1115/OMAE2021-62827.

[77] N. Alharthy, T. Teklu, H. Kazemi, R. Graves, S. Hawthorne, J. Braunberger, B. Kurtoglu, Enhanced Oil Recovery in Liquid-Rich Shale Reservoirs: Laboratory to Field, SPE Res. Eval. Eng. 21 (2017) 137–159, https://doi.org/10.2118/175034-PA.

[78] E. Behzadfar, S.G. Hatzikiriakos, Diffusivity of CO2 in bitumen: pressure−decay measurements coupled with rheometry, Energy Fuels 28 (2014) 1304–1311, https://doi.org/10.1021/ef402392r.

[79] T.A. Renner, Measurement and correlation of diffusion coefficients for CO2 and rich-gas applications, SPE Reservoir Eng. 3 (1988) 517–523, https://doi.org/10.2118/15391-PA.

[80] D. Unatrakarn, K. Asghari, J. Condor, Experimental studies of CO2 and CH4 diffusion coefficient in bulk oil and porous media, Energy Procedia 4 (2011) 2170–2177, https://doi.org/10.1016/j.egypro.2011.02.103.

[81] A. Kavousi, F. Torabi, C.W. Chan, E. Shirif, Experimental measurement and parametric study of CO2, solubility and molecular diffusivity in heavy crude oil systems, Fluid Phase Equilib. 371 (2014) 57–66, https://doi.org/10.1016/j.fluid.2014.03.007.

[82] S. Li, Z. Li, Q. Dong, Diffusion coefficients of supercritical CO2 in oil-saturated cores under low permeability reservoir conditions, J. CO2 Utiliz. 14 (2016) 47–60, https://doi.org/10.1016/j.jcou.2016.02.002.

[83] J. Yao, Y. Gu, A new experimental method for measuring the bubble-point pressures of the light crude oil–CO2 system at different CO2 concentrations, Fuel 311 (2022) 122526, https://doi.org/10.1016/j.fuel.2021.122526.

[84] M.G. Rezk, J. Foroozesh, Phase behavior and fluid interactions of a CO2-Light oil system at high pressures and temperatures, Heliyon 5 (2019) e02057.

[85] K. Zhang, L. Tian, L. Liu, A new analysis of pressure dependence of the equilibrium interfacial tensions of different light crude oil–CO2 systems, Int. J. Heat Mass Transf. 121 (2018) 503–513, https://doi.org/10.1016/j.ijheatmasstransfer.2018.01.014.

[86] H. Li, S. Zheng, D. Yang, Enhanced swelling effect and viscosity reduction of solvent(s)/CO2/heavy-oil systems, SPE J. 18 (2013) 695–707, https://doi.org/10.2118/150168-PA.

[87] D.J. Graue, E.T. Zana, Study of a possible CO2 flood in rangely field, J. Pet. Technol. 33 (1981) 1312–1318, https://doi.org/10.2118/7060-PA.

[88] J.R. Welker, Physical properties of carbonated oils, J. Pet. Technol. 15 (1963) 873–876, https://doi.org/10.2118/567-PA.

[89] K.N. Jha, A laboratory study of heavy oil recovery with carbon dioxide, J. Can. Pet. Technol. 25 (1966) 54–63, https://doi.org/10.2118/86-02-03.

[90] M.E. Perez-Blanco, E. Maginn, Molecular dynamics simulations of CO2 at an ionic liquid interface: adsorption, ordering, and interfacial crossing, J. Phys. Chem. B 114 (2010) 11827–11837.

[91] L. Zhao, S. Lin, J.D. Mendenhall, P.K. Yuet, D. Blankschtein, Molecular dynamics investigation of the various atomic force contributions to the interfacial tension at the supercritical CO2-water interface, J. Phys. Chem. B 115 (2011) 6076–6087.

[92] F.M. Orr, J.P. Heller, J.J. Taber, Carbon dioxide flooding for enhanced oil recovery: promise and problems, J. Am. Oil Chem. Soc. 59 (1982) 810A–A817, https://doi.org/10.1007/BF02634446.